Response to reviewers

We thank both reviewers for their useful comments on our paper. Please note that all line numbers refer to the version with *tracked changes*.

Reviewer #1

Significant comments:

However, I am very concerned whether their results are not unduly influenced - or even artefact - of the way they initialize their trajectory model.

If the initiation level is indeed 370K (and this is not a typo), then the model is essentially initialized with the driest possible state in the colder regions (over the cold Western Pacific, the tropopause is around 370K), and it is trivial that the model has a dry bias below that level - which is a problem particularly for the 100hPa level. (I should add that the display of data on pressure levels - necessary for MSL - makes it very difficult for the reader to understand whether the model is initialized above or below that pressure level.) Above 370K, this model may have trajectories that never experienced a true cold point, but the biggest problem is below that level: in this model, anything below 370K is populated only by descending pathways - and none have just directly come up from the troposphere (which can be expected to be at local saturation, and hence much moister). This most certainly biases the results strongly.

The serious concerns with the initialization preclude further discussion of the results since the quantitative numbers for convective moistening may be strongly affected. This paper tackles an important problem, but the authors need to demonstrate that their results are not unduly influenced by the initialization - which should be done in the troposphere and not at the tropopause. Major revisions are therefore inevitable, unfortunately.

This is a good point. We have re-run all the trajectory models with parcels initialized at 360 K. The 360-K potential temperature is above the average level of zero heating rates and below the cold point level, so parcels will ascend upon initialization and experience the cold point. For MERRA-2, the average heating rates below ~365 K in the NH subtropics are negative. To deal with this problem, we released those parcels above the level of zero heating rates for MERRA-2 simulations. See detailed information on our new initialization at 360 K (Section 2.4, Lines 218-255).

We have updated all our trajectory results (Figures 1-2 and Figures 5-9) and discussion accordingly throughout the paper.

While some quantitative details of the analyses have changed, our conclusion is unchanged: The trajectory models are still unable to simulate the seasonal cycle in the NH subtropics when water vapor is influenced only by temperature; Our simulations still show that convective ice evaporation is important for the NH subtropical seasonal cycle.

Minor comments:

Further - are the authors really initializing the trajectories in the extratropical stratosphere up to 60 degrees latitude with 200ppmv as stated in the text? This seems dramatically off - I am puzzled how this would produce the (reasonably looking) patterns shown in Figure 5?

The answer is, yes, we initialize parcels well into mid-latitudes. The reason these parcels do not impact the 100-hPa water values is that most of these mid- and high-latitude parcels are descending, so they never reach 100 hPa. Any that do ascend and advected into the TTL are dehydrated by cold TTL temperatures, so their water vapor values are set by TTL temperatures by the time they get to 100 hPa. We have edited the texts in the paper to make sure that there is no confusion (Lines 214-217 and Lines 254-255).

Reviewer #2

Since this is mostly diagnosing an output result from the GEOSCCM I dont see what the pupose of the model runs done with ERAi and MERRA-2 add to this. I think figures 1 and 2 could have been made from just using trajectories driven from GEOSCCM thus simplifying the analysis and figures. I assume that driving the trajectory model with any of these wind and temperature fields will produce similar results. Ie compare figure 5 to 1 and 2. Maybe I just missed something here.

We disagree with this comment. Without the plots showing ERAi- and MERRA2-based trajectory simulations, our paper would be a model-only analysis. We would not be able to connect the GEOSCCM results with observations. The fact that the results produced by ERAi and MERRA2 trajectory without convection look similar to those from the GEOSCCM trajectory without convection is a key link in the chain of logic of our paper. Thus, we will leave the figures in.

On page 11 line 325 it –> in.

We have updated the text. (Line 764)

Impact of convectively lofted ice on the seasonal cycle of water vapor in the tropical tropopause layer

Deleted: tropical lower stratospheric

Xun Wang[1], Andrew E. Dessler[1], Mark R. Schoeberl[2], Wandi Yu[1], and Tao Wang[3]

[1]Department of Atmospheric Sciences, Texas A&M University, College Station, TX, USA
[2]Science and Technology Corporation, Columbia, MD, USA
[3]University of Maryland, College Park, MD, USA

Correspondence to: Andrew E. Dessler (adessler@tamu.edu)

Abstract. We use a forward Lagrangian trajectory model to diagnose mechanisms that produce water vapor seasonal cycle observed by the Microwave Limb Sounder (MLS) and reproduced by the Goddard Earth Observing System Chemistry Climate Model (GEOSCCM) in the tropical tropopause layer (TTL). We confirm in both the MLS and GEOSCCM that the seasonal cycle of water vapor entering the stratosphere is primarily determined by the seasonal cycle of TTL temperatures. However, we find that the seasonal cycle of temperature predicts a smaller seasonal cycle of TTL water vapor between 10°N-40°N than observed by MLS or simulated by the GEOSCCM. Our analysis of the GEOSCCM shows that including evaporation of convective ice in the trajectory model increases both the simulated maximum value of the 100-hPa 10°N-40°N water vapor seasonal cycle as well as increasing the seasonal-cycle amplitude. We conclude that the moistening effect from convective ice evaporation in the TTL plays a key role regulating and maintaining seasonal cycle of water vapor in the TTL. Most of the convective moistening in the 10°N-40°N range comes from convective ice evaporation occurring at the same latitudes. A small contribution to the moistening comes from convective ice evaporation occurring between 10°S-10°N. Within the 10°N-40°N band, the Asian monsoon region is the most important region for convective moistening by ice evaporation during boreal summer and autumn.

Deleted: the tropical lower stratospheric (LS)

Deleted: LS

Deleted: . We show

Deleted: convectively lofted

Deleted: in

Deleted: by 1.9 ppmv (47%) and increases

Deleted: by 1.26 ppmv (123%), which improves the prediction of LS water vapor annual cycle

Deleted: the tropical LS water vapor

Deleted: and convective moistening

1 Introduction

Stratospheric water vapor is important for the radiative budget of the atmosphere and the regulation of stratospheric ozone (e.g., Solomon et al., 1986; Dvortsov and Solomon, 2001). One of the key features of the tropical lower stratospheric (LS) water vapor is its seasonal cycle often referred to as the "tape recorder" (Mote et al., 1995, 1996). The amount of water vapor entering the stratosphere and its seasonal cycle is primarily controlled by temperatures in the tropical tropopause layer (TTL) (Brewer, 1949; Holton et al., 1995; Fueglistaler et al., 2009). The low TTL temperatures freeze-dry the air, reducing the water vapor mixing ratios and imprinting the seasonal cycle on air ascending into the stratosphere through the TTL (e.g., Mote et al., 1996; Fueglistaler, 2005; Schoeberl et al., 2008; Fueglistaler et al., 2009).

Deleted: 1 Introduction
Stratospheric water vapor is important for the radiative budget of the atmosphere and the regulation of stratospheric ozone (e.g. Solomon et al., 1986; Dvortsov and Solomon, 2001). One of the key features of the tropical lower stratospheric (LS) water vapor is its seasonal cycle often referred to as the "tape recorder" (e.g. Mote et al., 1995, 1996). The amount of water vapor entering the stratosphere and its seasonal cycle is primarily controlled by temperatures in the tropical tropopause layer (TTL) (e.g. Brewer, 1949; Holton et al., 1995; Fueglistaler et al., 2009). The low TTL temperatures freeze-dry the air, reduce the water vapor mixing ratio to local saturation, and imprint the seasonal cycle on air ascending into the stratosphere (e.g. Mote et al., 1996; Fueglistaler, 2005; Schoeberl et al., 2008; Fueglistaler et al., 2009).

Analyses of observations have suggested that deep convection reaching the TTL may also be important for regulating the

Deleted: is

amount of water vapor entering the stratosphere. Nielsen et al. (2007) and Corti et al. (2008) suggested that deep penetrating convection deposits ice particles above the cold point tropopause, where ice may evaporate and cause a moistening effect. This idea is also supported by observations of enrichment of the deuterated isotopologue of water vapor (HDO) in the tropical LS (Moyer et al., 1996; Dessler et al., 2007; Steinwagner et al., 2010). The role of convective ice evaporation in the stratospheric entry water vapor has also been addressed in several model studies. Schoeberl et al. (2014, 2018, 2019) quantified the global impact of convective ice on winter 2008/2009 water vapor between 18-30 km, and concluded that, for global average water vapor between 18-30 km during winter, the convective ice evaporation plays a small role, since convection rarely reach the level of the tropopause cold point. During El Niño events, convective ice evaporation appears to play a larger role in the interannual variability of TTL and LS water vapor (Avery et al., 2017; Ye et al., 2018). On longer time scales, convective ice evaporation was found to contribute to an important fraction of the increase of stratospheric entry water vapor over the next century in two chemistry-climate models (Dessler et al., 2016).

The goal of this paper is to investigate the impact of convective moistening on the seasonal cycle of water vapor entering the stratosphere. Previous analyses have separately investigated the winter/summer impact, interannual variability, and the long-term trend (Ueyama et al., 2015, 2018; Dessler et al., 2016; Avery et al., 2017; Schoeberl et al., 2014, 2018; Ye et al., 2018). However, less work has been done on understanding the impact of convective ice on the seasonal cycle. The basics of the water vapor seasonal cycle can be understood simply: more water vapor enters the LS during boreal summer, when TTL temperatures are generally higher and vice versa during boreal winter. Observations (Fig. 1a-c) reveal that zonal mean water vapor is observed to have a larger amplitude seasonal cycle in the NH subtropics near the tropopause level (e.g., Rosenlof, 1997; Randel et al., 1998, 2001, and references therein), despite the fact that the temperature seasonal cycle is symmetric about the equator (Figs. 1b-c). We will refer to this as "the hemispheric asymmetry". At higher altitudes, the hemispheric asymmetry gradually disappears (Fig. 1a) (e.g., Randel et al., 1998, 2001).

Previous studies have suggested that this hemispheric asymmetry structure in the water vapor seasonal cycle is due to processes within the Southeast Asian monsoon and North American monsoon region, including both diabatic and adiabatic transport in the TTL (Rosenlof, 1997; Randel et al., 1998; Dethof et al., 1999; Bannister et al., 2004; Gettelman et al., 2004; Pan et al., 1997, 2000, Park et al., 2004, 2007; Wright et al., 2011; Ploeger et al., 2013). Indeed, the MLS data (Fig. 2c) show that the summertime maxima of the 100-hPa water vapor is confined in the Asian monsoon and North American monsoon anti-cyclones (Rosenlof, 1997; Jackson et al., 1998; Randel et al., 1998, 2001; Dessler and Sherwood, 2004; Randel and Park, 2006; Park et al., 2007; Bian et al., 2012) and become weaker above 100 hPa (Figs. 2a-b).

Many previous studies have investigated impact of convection within the monsoon regions on the budget of the stratospheric entry water vapor. Dessler and Sherwood (2004) used a budget model with and without convection and concluded that, during summer, moistening by deep penetrating convection increases the northern hemisphere (NH) extratropical water vapor at 380-K isentrope by 40%. Fu et al. (2006) suggested that the deep convection over the Tibetan Plateau acts as a short circuit of water

Deleted: , which suggests moistening by evaporated convective cloud ice

Deleted: Dessler and Sherwood (2004) used simple budget models with and without convection and concluded that, during summer, moistening by deep penetrating convection increases the northern hemisphere extratropical water vapor at 380-K isentrope by 40%. Ueyama et al. (2015) included convective ice evaporation in the trajectory model simulation with observed convective cloud top and concluded that convection moistens the 100 hPa level by 0.3 ppmv in boreal winter (which is less than 10%). Schoeberl et al. (2014, 2018)

Deleted: only

Deleted: They suggested that warmer temperatures or higher penetrating convection may result in more hydration from the convection ice evaporation.

Deleted: entering the stratosphere

Deleted: is

Deleted: LS

Deleted: The goal of this paper is to investigate the impact of convective ice on the seasonal cycle of water vapor in the TTL and LS. Previous analyses have focused on global impact, interannual variability, and the longterm trend (e.g. Ueyama et al., 2015; Dessler et al., 2016; Avery et al., 2017; Schoeberl et al., 2014, 2018; Ye et al., 2018). However, there is a strong seasonal cycle in LS water vapor and less work has been done on understanding the impact of convective ice. The basics of the water vapor seasonal cycle can be understood simply: more water vapor enters the LS during boreal summer, when TTL temperatures are generally higher and vice versa during boreal winter. But closer examination of the data reveals some deficiencies in this simple picture. Figures 1b-c show the MLS seasonal cycle of water vapor. At 100 hPa and 82.5 hPa, the zonal mean water vapor is observed to have maximum seasonal oscillation in the northern hemispheric subtropics (e.g. Rosenlof, 1997; Randel et al., 1998, 2001, and references therein) despite the fact that the temperature seasonal cycle is symmetric about the equator (Figs. 1b-c). As water vapor is transported further upward, the hemispheric asymmetry feature in the seasonal cycle gradually disappears (Fig. 1a) (e.g. Randel et al., 1998, 2001). The lower altitude hemispheric asymmetry indicates that processes other than dehydration by large-scale TTL temperatures may play a role in the LS water vapor budget. ¶
Previous studies have suggested that this hemispheric asymmetry structure in the water vapor seasonal cycle is due to processes within the Southeast Asian monsoon and North American monsoon region, including both diabatic and adiabatic transport in the TTL and lowermost stratosphere (e.g. Rosenlof, 1997; Randel et al., 1998; Dethof et al., 1999; Bannister et al., 2004; Gettelman et al., 2004; Pan et al., 1997, 2000, Park et al., 2004, 2007; Wright et al., 2011; Ploeger et al., 2013). Indeed, the MLS data (Fig. 2c) show that the summertime maxima of the LS water vapor is confined in the Asian monsoon and North American monsoon anti-cyclone at 100 hPa (e.g. Rosenlof, 1997; Jackson et al., 1998; Randel et al., 1998, 2001; Dessler and Sherwood, 2004; Randel and Park, 2006; Park et al., 2007; Bian et al., 2012) and become weaker above 100 hPa (Figs. 2a-b). ¶
Other studies have investigated impact of convectively injected water vapor and overshooting deep convection within the monsoon regions on the budget of the topical LS water vapor.

vapor ascending across the tropical tropopause. James et al. (2008) used a trajectory model and concluded that air parcels are lifted by convection over Southeast Asia and then transported into the TTL by the monsoon anticyclone, avoiding the cold pool in the deep tropics. However, they pointed out that direct convective injection has a limited impact on the 100-hPa water vapor budget, contributing to 0.3 ppmv of the water vapor in the Asian monsoon region. Schwartz et al. (2013) provided evidence of occasional enhanced 100-hPa and 82.5-hPa water vapor by convective injection over the Asian and North American monsoon regions using satellite observations. Randel et al. (2015) investigated subseasonal variations in 100-hPa water vapor in NH monsoon regions and suggested that stronger convection leads to lower TTL temperatures in the monsoon regions, which results in less LS water vapor there, thereby concluding that the LS water vapor in the monsoon regions is mainly controlled by large-scale transport and TTL temperatures there. Ueyama et al. (2018) investigated the convective moistening effect on 100-hPa water vapor during boreal summer. They used a trajectory model that includes cloud formation, gravity waves, and convective moistening and concluded that convection moistens the water vapor averaged over 10°S-50°N by 0.6 ppmv (~15%) and that convective moistening over the Asian monsoon region plays an important role.

Deleted: , using

Deleted: , suggested

Deleted: lowermost stratospheric

Deleted: LS

Deleted: the northern hemisphere

The role of convective ice evaporation in the TTL during boreal summer is still under debate. Furthermore, it's impact on the TTL water vapor seasonal cycle has not been fully explored. In this study, we quantitatively investigate the impact of convective ice evaporation on the seasonal cycle of water vapor in the TTL.

Deleted: tropical LS

Deleted: , however,

Deleted: The seasonal cycle is one of the key features of the tropical LS water vapor, so it is important that we fully understand the mechanisms that drive it.

Deleted: test whether moistening by

Deleted: is playing a role

Deleted: tropical LS water vapor seasonal cycle

2 Models and Data

2.1 MLS water vapor

We analyze here version 4.2 level 2 water vapor retrieved from the Earth Observing System (EOS) Microwave Limb Sounder (MLS) instrument on the Aura spacecraft (Livesey et al., 2017). Since August 2004, the MLS provides ~3500 vertical scans of the earth's limb from the surface to 90 km each day, covering a latitude range of 82°S to 82°N with a horizontal resolution of 1.5°along the orbit track (Lambert et al., 2007). The MLS water vapor retrieval has a vertical resolution of about 3 km in the TTL, with precision at 100 hPa and 82.5 hPa of 15% and 7%, respectively. The accuracy of the water vapor at 100 hPa and 82.5 hPa is 8% and 9%, respectively (Livesey et al., 2017). We composite the daily standard water vapor between August 2004 to October 2018 to produce monthly means on a horizontal grid of 4° latitude by 8° longitude following the data-screening in Livesey et al., (2017).

Deleted: analyse

Deleted: mean averaged

2.2 Ice Water Content from Cloud-Aerosol Lidar with Orthogonal Polarization

The Cloud-Aerosol Lidar with Orthogonal Polarization (CALIOP) is a two-wavelength polarization elastic backscatter lidar that detects global tropospheric and lower stratospheric aerosol and cloud profiles (Hu et al., 2009; Liu et al., 2009; Vaughan et al., 2009; Winker et al., 2009, 2010; Young and Vaughan, 2009; Avery et al., 2012; Heymsfield et al., 2014). We use the CALIOP Level 2 Cloud Profile Product in version 4.2, with horizontal resolution of 5 km along-track and 60 m vertically in the TTL and LS. The CALIOP cloud Ice Water Content (IWC) is derived from a parameterized function of the CALIOP 532 nm cloud particle extinction profiles (Avery et al., 2012; Heymsfield et al., 2014). We use the IWC from all clouds minus the IWC from thin cirrus clouds (clouds that are not opaque) above 146 hPa, which is a rough estimate of convective ice in the TTL region, since the CALIOP does not separate convective from non-convective IWC measurements. These CALIOP IWC data, obtained between May 2008 and December 2013, are then monthly averaged onto the same horizontal and vertical grids as were used for the MLS data.

2.3 GEOSCCM

We also analyze simulations from the Goddard Earth Observing System Chemistry Climate Model (GEOSCCM). The GEOSCCM couples the GEOS-5 general circulation model (Rienecker et al., 2008; Molod et al., 2012) to a comprehensive stratospheric chemistry module (Oman and Douglass, 2014; Pawson et al., 2008). The GEOSCCM uses a single-moment cloud microphysics scheme (Bacmeister et al., 2006; Barahona et al., 2014). The run analyzed here starts in 1998 and ends in 2099 and driven by the Representative Concentration Pathway (RCP) 6.0 greenhouse gas scenario (Van Vuuren et al., 2011) and the A1 scenario for ozone depleting substances (World Meteorological Organization, 2011). Sea surface temperatures and sea ice concentrations were prescribed from Community Earth System Model version 1 simulations (Gent et al., 2011). The model has a horizontal resolution of 2°latitude by 2.5°longitude and 72 vertical levels up to the model top at 0.01 hPa (Molod et al., 2012).

2.4 Trajectory Model

We also use the forward, domain filling, diabatic trajectory model described in Schoeberl and Dessler (2011) and updated in subsequent publications. The trajectory model uses 6-hourly instantaneous horizontal winds and 6-hourly average diabatic heating rates to advect parcels using the Bowman trajectory code (Bowman, 1993; Bowman and Carrie, 2002). Meteorological fields used to drive the model in this paper come from the European Centre for Medium-Range Weather Forecasts (ECMWF) ERA-interim (ERAi), and Modern-Era Retrospective analysis for Research and Applications-2 (MERRA-2) (Molod et al., 2015; Gelaro et al., 2017), and the GEOSCCM.

In this study, the trajectory model initializes 1350 parcels daily in the upper troposphere on an equal area longitude-latitude grid covering 0-360°longitude and ± 60°latitude, and with initial water vapor mixing ratio of 200 parts per million by volume (ppmv). This value is well above saturation, so the parcels are dehydrated to saturation after the first time step of the trajectory model run. Sensitivity tests show that our results are not impacted by the initialization values.

The initialization level is at 360-K potential temperature, which is above the average level of zero heating (~355-360 K) (Fueglistaler et al., 2009) but below the tropical cold point. In the MERRA-2, the average heating rates below ~365 K in the NH subtropics are negative during boreal summer (not shown), which results in parcels in that region immediately

Deleted: ice

Deleted: detected by the CALIOP

Deleted: In this study, we average

Deleted: interpolate the CALIOP IWC into

Deleted: gridded fields on pressure levels using data from 2007 to 2017.

Deleted: of the TTL and LS

Moved down [1]: here starts in 1998 and ends in 2099 and driven by the Representative Concentration Pathway (RCP) 6.0 greenhouse gas scenario (Van Vuuren et al., 2011) and the A1 scenario for ozone depleting substances (World Meteorological Organization, 2011). Sea surface temperatures and sea ice concentrations were prescribed from Community Earth System Model version 1 simulations (Gent et al., 2011). The model has a horizontal resolution of 2°latitude by 2.5°longitude and 72 vertical levels up to the model top at 0.01 hPa (Molod et al., 2012).

Deleted: The run analysed

Deleted: The GEOSCCM uses a single

Moved (insertion) [1]

Deleted: The convective IWC in the GEOSCCM originates in moist detraining convection, which uses Relaxed Arakawa-Schubert convective parameterization (Moorthi and Suarez, 1992).

Deleted: In this study, we

Deleted: , from a variety of sources such as

Deleted: dimensionless

Deleted: 370

Deleted: tropopause (~380 K).

descending back to the troposphere after initialization. To deal with this problem, we initialize parcels at 360 K in MERRA-2 simulations. But if the local heating rate at 360 K is negative, we raise the initialization level to the lowest isentropic level with positive heating rate at the same horizontal position. However, we note that the level of zero heating rate is higher (~370 K) over the NH monsoon regions in MERRA-2. Releasing parcels at ~370 K over the NH monsoon regions results in insufficient dehydration and a moist bias there (Schoeberl et al., 2013; Ueyama et al., 2018). To avoid this bias, we set the local initialization level to 366 K (1 K above the tropical average level of zero heating rate) for those parcels. At the end of each day, parcels below the 250-hPa pressure surface or above the 5000-K isentrope are removed because they are considered outside of the model boundaries. We note that the parcels initialized at mid-latitudes mostly descend into the troposphere.

Along each trajectory, an instant dehydration scheme is used. In this scheme, anytime the relative humidity (hereafter RH, always with respect to ice) exceeds the dehydration threshold, water vapor is instantly removed to reduce the parcel's RH to the dehydration threshold. The RH calculation uses 6-hourly temperatures linearly interpolated in time and space to parcel locations at each time step; the RH is computed using the saturation mixing ratio at that temperature Murphy and Koop (2005). The pre-set dehydration threshold is 100% RH for the ERAi trajectory runs and MERRA-2 trajectory runs. For the GEOSCCM trajectory runs, the pre-set dehydration threshold is 80% RH, since in the GEOSCCM dehydration occurs when the grid-average RH is around this value (Molod et al., 2012). The same parameterization for the pre-set RH threshold of 80% was used successfully analyzing the water vapor interannual variability in the GEOSCCM in Dessler et al. (2016) and Ye et al. (2018). We will refer to this version as the "standard" trajectory model – another version that includes ice evaporation will be introduced later.

As an alternative to instant dehydration we can run a cloud model along the trajectory model, which is described in Schoeberl et al. (2014). The cloud model triggers ice nucleation at a prescribed nucleation RH (NRH) threshold and the number of ice particles produced upon nucleation is proportional to the parcel cooling rate using the relationship derived by Kärcher et al. (2006). The ice mixing ratio is carried with the parcel along with number of crystals and size. Ice crystal distribution has a single size mode that varies as the parcels grow or sublimate. Gravitational sedimentation reduces the total ice amount within the parcel. Ice crystals are assumed to be spheres which is reasonable for small crystals in the upper troposphere (Woods et al., 2018). The cloud model uses a fixed cloud geometrical thickness of 500 m based on the TTL cloud thickness distribution observed by CALIOP (Schoeberl et al., 2014). We also assume that ice falling out of the cloud slowly sublimates in sub-saturated layers well below the cloud. The cloud model incorporates more realistic physics than the instant dehydration scheme we use in the standard trajectory model and it produces good agreement with observational data from aircraft flights (Schoeberl et al., 2015). The physics in the cloud model has a net effect of slowing down the parcels' dehydration rate and increasing water vapor in the LS compared to the instant dehydration scheme (Schoeberl et al., 2014).

Deleted: Along each trajectory, an instant dehydration scheme is used. In this scheme, anytime the RH (with respect to ice) exceeds the dehydration threshold, water vapor is instantly removed to reduce RH to the dehydration threshold. The pre-set dehydration threshold is 100% RH for the ERAi trajectory runs and MERRA-2 trajectory runs. For the GEOSCCM trajectory runs, the pre-set dehydration threshold is 80% RH, since in the GEOSCCM dehydration occurs when the grid-average RH is around this value (Molod et al., 2012). The same parameterization for the pre-set RH threshold of 80% was used successfully to analyse the GEOSCCM in Dessler et al. (2016) and Ye et al. (2018), which produces water vapor in good agreement with the observations. In all trajectory runs, the parcel temperature is calculated by linearly interpolating 6-hourly temperatures in time and space to parcel locations at each time step; the RH is computed using the saturation mixing ratio at that temperature (Murphy and Koop, 2005). The trajectory model includes methane oxidation as a water source as described in Schoeberl and Dessler (2011), but this process is unimportant in the TTL and LS. We will refer to this version as the "standard" trajectory model – another version that includes ice evaporation will be introduced later.¶

Deleted: use

Deleted:

Deleted: The cloud model

Deleted: The cloud model incorporates more realistic physics than the instant dehydration scheme we use in the standard trajectory model.

All the trajectory model runs include methane oxidation as a water source as described in Schoeberl and Dessler (2011), but this process is unimportant in the TTL and LS. We start all trajectory models on 1/1/2000 and analyze the model results from 2005 to October 2018, so that we can compare the ERAi and MERRA-2 driven trajectory results to the MLS observations. The GEOSCCM is a free-running model, so interannual variability of the model will not match MLS observations. We will therefore compare a multi-year average of the GEOSCCM to observations.

Deleted: the

Deleted: results from

3 Results

3.1 Impact of convective moistening on the seasonal cycle

Figures 1d-i show the water vapor seasonal cycle at 100 hPa, 82.5 hPa, and 68 hPa simulated by the standard trajectory model driven by ERAi, and MERRA-2 in which dehydration is entirely driven by temperature and there is no convective influence (See Table 1 for summary of the trajectory model cases). To compare with the MLS, we averaged the trajectory water vapor fields in the vertical using the MLS averaging kernels following the instructions from Livesey et al. (2017). The trajectory models fail to produce the hemispheric asymmetry, the larger water vapor seasonal cycle in the NH subtropics in August-September at 100 hPa and 82.5 hPa (Figs. 1e-f and 1h-i). Specifically, the ERAi and MERRA-2 trajectory models underestimate the 100-hPa seasonal amplitude over 10°N-40°N by 0.5 ppmv (24%) and 0.89 ppmv (43%) respectively. At 68 hPa, the trajectory models agree with the MLS that the seasonal cycle is approximately centered over the equator, although they underpredict the MLS (Figs. 1a, 1d, and 1g). During June-July-August (JJA) (Figs. 2d-i), the trajectory models underestimate the maxima over the Asian and North American monsoon regions (Figs. 2e-f, 2h-i), which agrees with Ueyama et al. (2018) who also showed that the trajectory model driven by the ERAi without any convective influence fails to reproduce the boreal summer maxima. At 68 hPa, the monsoonal maxima are nearly gone (Figs. 2d and 2g).

Deleted: Unlike the MLS observations, the

Deleted: maximum

Deleted: values

Deleted: northern hemisphere

Deleted: it underpredicts

Deleted: 2e, 2f, 2h, and 2i). At 68 hPa, the monsoonal maxima are nearly gone and the trajectory models do a reasonable job of simulating the spatial patterns (Figs.

We also ran the ERAi and MERRA-2 simulation with the cloud model described in Section 2.4 operating along the trajectory model, with 100% NRH (Table 1). Note that this version of the trajectory model does not have any convective ice in it, so water vapor is still regulated entirely by TTL temperatures. Figures 1j-o show that the cloud model produces larger water vapor values in the seasonal cycles at 100 hPa, 82.5 hPa, and 68 hPa. There is also a slight increase in the seasonal maximum poleward of 20°N (Figs 1l and 1o) at 100 hPa. The ERAi and MERRA-2 trajectory models with the cloud model increase the 10°N-40°N seasonal amplitude at 100 hPa by 0.1 ppmv (6%) and 0.08 ppmv (7%) - a small improvement compared to the instant dehydration scheme. However, the cloud model doesn't help reproduce the observed hemispheric asymmetry in the seasonal cycles at 100 hPa and 82.5 hPa – it basically increases water vapor both north and south of the equator. During JJA (Figs. 2l and 2o), the cloud model increases the 100-hPa water vapor values over the Asian monsoon and North American monsoon regions, but there is still an underestimation compared to the MLS. We note that the NRH threshold of 100% can be too low, since previous observations showed that the NRH can be as high as 160%-170% in the TTL region during winter

Deleted: However, the cloud model doesn't help reproduce the hemispheric asymmetry feature in the seasonal cycles at 100 hPa and 82.5 hPa – it basically increases water vapor both north and south of the equator. During JJA (Figs. 2l and 2o), the cloud model helps reproduce the 100-hPa water vapor maxima over the Asian monsoon and North American monsoon regions, but it results in overestimated water vapor values over the Southern hemispheric subtropics. Thus, regardless of dehydration scheme, models that regulate water vapor only through TTL temperatures and large-scale transport do not reproduce important features of the TTL/LS water vapor seasonal cycle, including the observed hemispheric asymmetry.

(Jensen et al., 2013). Schoeberl et al. (2016) showed that the sensitivity of trajectory simulated water vapor to the NRH threshold is 0.1-0.2 ppmv per 10 percent NRH, and that an NRH threshold of 140-145% in the trajectory model produces water vapor in better agreement with the MLS observations during winter. However, our result regarding the hemispheric asymmetry and boreal summer maxima agrees with Ueyama et al. (2018), who set the NRH threshold to 160%, indicating that the hemispheric asymmetry is not sensitive to the choice of NRH threshold. Thus, regardless of dehydration scheme, models that regulate water vapor only through TTL temperatures and large-scale transport do not reproduce important features of the 100 – 82.5 hPa water vapor seasonal cycle, including the observed hemispheric asymmetry.

Our hypothesis is that convective moistening is causing the hemispheric asymmetry in the TTL water vapor seasonal cycle. Previous analyses (e.g., Ueyama et al., 2018) have attempted to test this idea by directly incorporating observed convection into the trajectory model and then evaluating how agreement with water vapor observations improved. However, estimating convective height from passive infrared measurements is difficult and Ueyama et al. (2018) noted that errors in the convective heights created issues in their analysis. Given this significant uncertainty in an observation-only approach, we therefore take a different tack. We perform a parallel analysis with the GEOSCCM, a model that we show below reproduces the hemispheric asymmetry and we will examine the causes of the asymmetry in that model and then evaluate whether we think that is what is going on the real world.

Deleted: To

Deleted: , we

Deleted: where evaporation of convective ice is known to add water to the TTL (Dessler et al., 2016; Ye et al., 2018).

In our analysis, we first run the standard trajectory model driven by meteorology from the GEOSCCM which, like the standard models analyzed above, uses instant dehydration to regulate water vapor exclusively through TTL temperatures. We also run a second version of the trajectory model, the "ice model", in which we add the convective moistening to the trajectory model.

Deleted: experiment

Deleted: analysed

Deleted: evaporation of convectively lofted ice

The GEOSCCM outputs convective ice at every step. To add convective moistening to our trajectory model, we linearly interpolate the GEOSCCMs' 6-hourly three-dimensional convective ice field to the location and time of each trajectory's time step. Then, at each time step, we assume complete evaporation of the ice into the sub-saturated parcels by adding the ice water content to the parcels' water vapor — although we do not let parcels exceed the pre-set RH threshold of 80%. This is similar to the convective moistening scheme used by Schoeberl et al. (2014), who used MERRA anvil ice to facilitate the convective moistening in the trajectory model. After each encounter, we do not allow parcels to carry any remaining convective ice downstream as Schoeberl et al. (2014) did in their ASC case. Ueyama et al. (2018) used a similar convective moistening scheme, where they saturated the column model up to the observed cloud top when a parcel's trajectory intersects a convective cloud. Because we assume instant dehydration and instant evaporation of the ice, we consider the convective moistening in our trajectory model runs to be an upper limit of the impact of convective ice evaporation on the TTL water content in the GEOSCCM (Dessler et al., 2016).

Deleted: the

Deleted: . To do that

Deleted: IWC

Deleted: this

Deleted: parcel

Deleted: GEOSCCM convective IWC

Deleted: parcel's

Deleted: Since

Deleted: this

Deleted: of

Deleted: TTL and LS

To test if GEOSCCM convective ice field is realistic, we compare GEOSCCM convective ice with CALIOP ice data (ppmv) (Figures 3 and 4). For the CALIOP, we show IWC from all clouds minus IWC from thin cirrus clouds (not opaque), above 146 hPa, which is a rough estimate of convective ice in the TTL region, although it is almost certainly an underestimate of true convective ice amount. There's general agreement between the spatial pattern of GEOSCCM and CALIOP convective ice. However, the GEOSCCM generally produces more convective ice and higher convective top altitudes than the CALIOP. To address these problems in the GEOSCCM, we also show the GEOSCCM convective ice field reduced by 80% (0.2ice), which brings tropical GEOSCCM convective ice into better agreement with the CALIOP values at 121 hPa and above (Figs. 3e-f and 4e-f). We show below two sensitivity tests that show our results are not sensitive to the overestimation of convective IWC and convective top altitude by the GEOSCCM.

The water vapor seasonal cycles from the GEOSCCM and various GEOSCCM trajectory model runs (Table 1) are shown in Fig. 5. These have been re-averaged in the vertical using the MLS averaging kernels (Livesey et al., 2017) to facilitate comparison with MLS. We focus on the 100-hPa level, where the hemispheric asymmetry is strongest. We note that the 100-hPa level is in the TTL and is not strictly above the tropopause, especially in the summer NH monsoon region. However, processes on this level play a key role in determining stratospheric water vapor (Fueglistaler et al., 2009).

The GEOSCCM reproduces the hemispheric asymmetry seen in the MLS observations (compare Fig. 5a with Fig. 1c), and shows that during JJA the 100-hPa water vapor maxima are located over the Asian monsoon and North American monsoon regions (compare Fig. 5b with Fig. 2c). The standard trajectory model driven by GEOSCCM meteorology, which regulates water entirely through TTL temperatures, does not reproduce the hemispheric asymmetry (Fig. 5c). That model also underestimates the JJA water vapor values in the Asian monsoon region and North American monsoon region (Fig. 5d). These results are similar to the comparison between MLS and the standard trajectory models driven by ERAi and MERRA-2 (Figs. 1f, 1i, 2f, and 2i)

Fig. 6 shows the 100-hPa water vapor seasonal cycles in the NH subtropics (10°N-40°N), deep tropics (10°S-10°N), and southern hemispheric subtropics (10°S-40°S). To aid in comparison, we have subtracted the annual mean from each data set. The standard model generally agrees well with the GEOSCCM and MLS in the 10°S-10°N and 10°S-40°S region (Figs. 6b-d). This suggests that the water vapor seasonal cycle in those regions is mainly controlled by the TTL temperatures and large-scale transport and implying that other factors, including convective ice evaporation, are less important. In the 10°N-40°N region, however, the standard model does a poor job, underestimating the MLS and GEOSCCM seasonal amplitude by 1.15 ppmv (55%) and 1.23 ppmv (57%) (Figs. 6a and 6d).

If we add convective ice evaporation to the trajectory model, then the models show a clear hemispheric asymmetry in the 100-hPa water vapor seasonal cycle and more pronounced seasonal maxima over the monsoon regions (Figs. 5e-h). Fig. 6 shows that the ice model and the 0.2ice model (the trajectory model where we add 0.2ice as shown in Figs. 3e-f) produce boreal

Deleted: In Figures 3 and 4

Deleted: IWC

Deleted: IWC. Note

Deleted: data includes all IWC, both convective and in situ, while GEOSCCM fields are for convection only.

Deleted: convective IWC

Deleted: IWC, which sets the groundwork for our

Deleted: moistening scheme. One clear difference is that

Deleted: IWC fields cover a narrower latitude range

Deleted: IWC (Fig. 3) – in particular, there is a tail of IWC in the CALIOP data in the DJF mid-latitudes that is missing in the GEOSCCM. Additionally,

Deleted: tends to have higher amounts of ice at each altitude level below about 100 hPa. The spatial pattern of CALIOP IWC (Fig. 4) is well reproduced by

Deleted: IWC, although the GEOSCCM generally has smaller values as expected since stratiform clouds aren't included in

Deleted: convective IWC.

Deleted: also

Deleted: The GEOSCCM agrees with the MLS (Fig. 1c) that the 100-hPa water vapor has a larger seasonal oscillation over 10°N-40°N than 10°S-40°S, and

Deleted: Figs. 5a-b).

Deleted: underestimates

Deleted: maximum values and amplitude of the GEOSCCM seasonal cycle in the northern

Deleted: subtropics by 1.3 ppmv (24%) and 1.15 ppmv (52%), respectively. It

Deleted: Figs. 5c-d

Deleted: Fig. 1f and 1i). The ice model, which includes evaporation of convective ice, shows a clear hemispheric asymmetry in the LS water vapor seasonal cycle and more pronounced seasonal maxima over the monsoon regions (Figs. 5e and 5f). Specifically, compared to the standard model, evaporation of convectively lofted ice increases the maximum value of the 10°N-40°N water vapor seasonal cycle by 1.9 ppmv (47%) in September.

Deleted: These results suggest that convective ice evaporation is important to the water vapor seasonal cycle in the northern hemispheric subtropics in the GEOSCCM. Dessler et al. (2016) analysed this same GEOSCCM run and showed that ice evaporation is required to accurately simulate the long-term trend in stratospheric water vapor. Our results are also similar to that obtained by Ye et al. (2018), who also analysed this GEOSCCM and showed that ice evaporation is required to reproduce the model's interannual variability of tropical LS water vapor. They found that the observed ... [1]

Deleted: northern hemispheric

Deleted: predicting an amplitude that is about half the amplitude ... [2]

Moved (insertion) [2]

Deleted: Fig.

summer and autumn water vapor values in the 10°N-40°N much closer to the GEOSCCM and MLS. The ice model and the 0.2ice model increase the 10°N-40°N seasonal maximum by 2.39 ppmv (63%) and 1.65 ppmv (44%), and increase the seasonal amplitude by 1.55 ppmv (169%) and 1.03 ppmv (112%) (Figs. 6a and 6d). This means convective ice evaporation is particularly important to the 100-hPa water vapor mixing ratio in NH subtropics during boreal summer and autumn, thereby playing a key role in the seasonal cycle there.

Fig5e shows that our ice model generates too much water vapor, consistent with too much IWC in the TTL. Given that the GEOSCCM's water vapor fields are reasonable (e.g., Fig. 5a vs. Fig. 1c), this further emphasizes that our instant dehydration model evaporates too much water vapor, thus yielding an upper limit of the impact of ice evaporation. It may also indicate a cancelling error in the GEOSCCM: too much water from ice cancelling a too low dehydration threshold (80%). Clearly, more research on this question is warranted.

Moved (insertion) [3]

Deleted: Fig.

Deleted: We note that the ice model does a good job reproducing the seasonal variations in the 10°N-40°N region (Fig. 6), but the absolute water vapor values it produced are generally overestimated compared to the GEOSCCM and MLS (Fig. 5). This is likely because the convective moistening scheme we used in the trajectory model instantly evaporates convective ice and hydrates parcels to the saturation threshold. We did another GEOSCCM trajectory analysis, in which we specify that evaporation relaxes the RH towards 80% with an e-folding time scale τ of 6 hours. Figures 5g-h show that this finite time ice evaporation scheme helps reduce the overestimation and produces water vapor values closer to the GEOSCCM. This reinforces the idea that the ice model we use in this paper provides an upper limit of the impact of convective ice evaporation on the water content of the TTL and LS (Dessler et al., 2016).

We ran another GEOSCCM trajectory ice model to test the sensitivity of water vapor at 100 hPa to convective ice altitude. This was in response to our observation that convective ice in the GEOSCCM went too high into the stratosphere compared to the CALIOP (Fig. 3a vs. Fig. 3c), and we wanted to see if this influences our results. In this test run, we do not allow any ice above the 90-hPa surface to evaporate, so that we eliminate any convective influence that is above that altitude. The zonal mean seasonal cycle and JJA water vapor at 100 hPa from this run is shown in Figs. 5i-j. The difference between the seasonal cycles from the ice model and this test run is less than 0.3 ppmv between 30°S – 30°N. The larger moisture difference at higher latitudes comes from convective moistening in the lowermost stratosphere. However, the hemispheric asymmetry is well reproduced by this test run. We thereby conclude that the impact of convective ice evaporation on the 100-hPa water vapor seasonal cycle is insensitive to convective ice occurrence that is too high in altitude.

These results suggest that convective ice evaporation in the TTL is important to the 100-hPa water vapor seasonal cycle in the NH subtropics in the GEOSCCM. Combined with the fact that the GEOSCCM has reasonable water vapor and convective fields, and that our results are insensitive to errors in the IWC amount and convective altitudes in the GEOSCCM, we believe this is a plausible explanation for the hemispheric asymmetry. That plausibility is strongly supported by the lack of a competing hypothesis for the asymmetry.

3.2 Source regions of convective ice evaporation

Our result begs the question of which region contributes most to this convective moistening? Here we define the quantity *net convective moistening* to be the water vapor mixing ratio in the ice model minus that in the standard trajectory model. The net convective moistening thus represents the net water vapor added by convective ice evaporation. In this section, we investigate the regional contribution to net convective moistening in the NH subtropics in the GEOSCCM, so we don't use the MLS averaging kernels in the vertical direction, as we did in Section 3.1. The net convective moistening in the NH subtropics

Deleted: Our results suggest that convective ice evaporation contributes an important part of the water vapor seasonal cycle in the 10°N-40°N region. This then

Deleted: We also quantify the rate of convective ice evaporation in the ice model.

seasonal maximum and seasonal amplitude is therefore 2.69 ppmv and 1.68 ppmv – slightly different from the values we show in Fig. 5. We also note that the 100-hPa net convective moistening value in the 10°S - 50°N domain produced by our GEOSCCM analysis during boreal summer is larger than the value of 0.6 ppmv produced by the observational analysis of Ueyama et al. (2018)'s observational analysis. This is because the combination of instant dehydration scheme and instant ice evaporation scheme we use in the trajectory model lead to larger net convective moistening. This also reinforces the idea that the ice model we use in this paper provides an upper limit of the impact of convective ice evaporation on the 100-hPa water content in the GEOSCCM (Dessler et al., 2016). Thus, we view our results to mainly be qualitatively useful.

We also quantify the *convective evaporation rate* in the ice model. To do this, we record the location and amount of water vapor added to each parcel from ice evaporation on every time step. We then grid and average these values to produce a three-dimensional field of the ice evaporation rate (in units of ppmv day^{-1}). Note that water vapor added by convection will not necessarily make it into the stratosphere — the added water vapor may be removed in subsequent dehydration events.

Fig. 7a and 7b show that convective evaporation rate generally follows the IWC. However, we see that the highest ice evaporation rates and net convective moistening (Fig. 7d) in regions where IWC is high and RH (Fig. 7c) is low (Dessler and Sherwood, 2004). In regions where both IWC and RH are high, evaporation is suppressed, and any air that is moistened by evaporation is rapidly re-dehydrated.

To determine how evaporation in different regions contribute to the 10°N-40°N seasonal cycle, we separately track the amount of water vapor produced by evaporation in specific latitude bands. Fig. 8 shows the seasonal cycle of net convective moistening at 100 hPa averaged in the 10°N-40°N region contributed by evaporation of convective ice between 10°N-40°N and 10°S-10°N. We note that, to obtain the net convective moistening and fractions contributed by specific latitude bands, we have not subtracted annual mean from the seasonal cycles in this plot like we did in Fig. 6.

During the winter (DJF), contributions from ice evaporation between 10°S-10°N and 10°N-40°N are about even, with slightly larger contribution from 10°S-10°N. During the summertime (JJA), however, evaporation of convective ice in the 10°N-40°N region is the dominant contributor to the net convective moistening. Specifically, it contributes to 63% (1.7 ppmv) and 59% (0.9 ppmv) of the net convective moistening in the 10°N-40°N water vapor seasonal maximum (September) value and seasonal amplitude, respectively. Convective ice evaporation between 10°S-10°N plays a smaller role, contributing to 31% (0.83 ppmv) and 17% (0.28 ppmv).

Next, we investigate net convective moistening in the 100-hPa 10°N-40°N water vapor seasonal cycle contributed by specific regions within the 10°S-40°N domain. To do this, we divide the 10°S-40°N domain into 12 equal-area boxes. We average the net convective moistening contributed by each of these boxes using the same method we used to calculate the contribution by

Deleted: 7a shows that from January to May, the convective IWC is abundant in the deep tropics between 20°S-20°N, but it doesn't produce large ice evaporation rates (Fig. 7b) or large net convective moistening (

Moved up [2]: Fig.

Deleted: 7d). This is a consequence of high RH during this period (Fig. 7c), which suppresses evaporation of convectively lofted ice. From June to September, on the other hand, RH is lower, so while there is less ice lofted in the TTL, it efficiently evaporates. This can be seen in Figs. 7b and 7d, which show maximum ice evaporation rates and net convective moistening during this time, located between 10°S-40°N, where the convective IWC is abundant. Between 10°S-40°S, however, there is little convective IWC available even though the RH is low, resulting in small evaporation rates and net convective moistening. Thus, the ice evaporation rate and net convective moistening are due to a combination of available convective IWC abundance and RH below saturation

Deleted: Both the ice

Deleted: rate and net convective moistening during June to September has maximum values between 10°N-40°N, which suggests that net convective moistening

Deleted: the 10°N-40°N water vapor seasonal cycle is largely contributed by local convective ice evaporation. But there is also a large evaporation rate between 10°S-10°N (

Moved up [3]: Fig.

Deleted: 7b). To determine if this tropical evaporation is contributing

Deleted: in the 10°N-40°N region that is

Deleted: of convective ice (net convective moistening) between 10°N-40°N and 10°S-10°N. Fig.

Deleted: absolute values of

Deleted: do

Deleted: subtract

Deleted: but during

Deleted: 46

Deleted: (71%)

Deleted: 1.09

Deleted: (86%)

Deleted: .

Deleted: 50

Deleted: (24.7%)

Deleted: 12

Deleted: (9.9%) of the net convective moistening in the 10°N-40°N water vapor seasonal maximum value and seasonal amplitude.

Deleted: calculate

10°N-40°N and 10°S-10°N. Fig. 9 shows the contribution from each box region to the net convective moistening in the 100-hPa 10°N-40°N water vapor seasonal maximum value in September and the seasonal amplitude.

We find that contribution from the box regions over Southeast Asia (10°N-40°N, 60°E-120°E), subtropical Western Pacific (10°N-40°N, 120°E-180°E), and North America (10°N-40°N, 120°W-60°W) dominate. The Southeast Asia region is most important, contributing to 20% (0.54 ppmv) and 20% (0.3 ppmv) of the net convective moistening in the 10°N-40°N water vapor seasonal maximum value and seasonal amplitude, respectively. This conclusion is consistent with Ueyama et al. (2018), who showed that parcels in the 10°S-50°N domain at 100 hPa are mainly hydrated by convection over Southeast Asia. Specifically, they showed that convection over the Asian monsoon region (0-40°N,40°E-140°E) contributes approximately 50% of the total convective moistening (10°S-50°N) at 100 hPa during August 2007. We computed the contribution from the same domain and got a contribution of 36%. The reason we produce a smaller contribution from this domain is that the GEOSCCM produces more convective ice over the tropical west Indian Ocean (Fig. 4), which results in larger convective moistening contributed by that region.

Deleted: contributes
Deleted: 56
Deleted: (27%)
Deleted: 37
Deleted: (30%)
Deleted: .

The subtropical Western Pacific also contributes to the net convective moistening in the 100-hPa 10°N-40°N water vapor seasonal cycle. This is due to the abundant convective ice over the subtropical west Pacific (Fig. 4b), which is likely related to the east-west oscillation of the Asian monsoon anticyclone (Pan et al., 2016; Luo et al., 2018). The North America region is less important in the ice model, contributing to 12% (0.3 ppmv) and 13% (0.21 ppmv) of the net convective moistening in the 10°N-40°N water vapor seasonal maximum value and seasonal amplitude. The GEOSCCM underestimates the observed convective ice over the North American monsoon above 120 hPa (not shown), which may cause the contribution from the North American region to be underpredicted.

Deleted: IWC
Deleted: 25
Deleted: (12%)
Deleted: 15
Deleted: (12%)
Deleted: This is because most of
Deleted: IWC in the GEOSCCM
Deleted: region is found below 100
Deleted:).

4 Summary

Deleted: Conclusion

In this study, we investigated mechanisms that drive the seasonal cycle of water vapor in the TTL. We use a Lagrangian trajectory model (Schoeberl and Dessler, 2011) to analyze the seasonal cycle in observations of water vapor made by the Microwave Limb Sounder (MLS) (Lambert et al., 2007; Livesey et al., 2017) as well as simulated fields from the Goddard Earth Observing System Chemistry Climate Model (GEOSCCM) (Rienecker et al., 2008; Molod et al., 2012; Pawson et al., 2008; Oman and Douglass, 2014).

Deleted: investigate
Deleted: TTL and tropical lower stratospheric (LS)
Deleted: analyse

Water vapor's seasonal cycle in the TTL and tropical lower stratosphere (LS), sometimes referred to as the "tape recorder," has highest values of water vapor entering the stratosphere during NH summer. We confirm in both the MLS observations and in the GEOSCCM that this is mainly due to the seasonal cycle of TTL temperatures. However, closer examination of the data reveals some deficiencies in this simple picture. Both the MLS and GEOSCCM show that the water vapor seasonal cycle in the TTL has a hemispheric asymmetry, with maximum seasonal cycle between 10°N-40°N, despite the fact that the TTL

Deleted: ,
Deleted: Northern Hemispheric
Deleted: tropical LS
Deleted: near the tropopause level

temperature seasonal cycle is symmetric about the equator (e.g., Rosenlof, 1997; Randel et al., 1998, 2001, and references therein). The hemispheric asymmetry is strongest at 100 hPa. Trajectory models that only regulate TTL and tropical LS water vapor using temperatures (Schoeberl and Dessler, 2011) from ERAi, MERRA-2, and GEOSCCM all produce weaker water vapor seasonal cycles between 10°N-40°N compared to the MLS and GEOSCCM. These indicate that the 100-hPa seasonal oscillation between 10°N-40°N is too large to be simply explained by TTL temperatures.

Recent studies suggested that evaporation of convective ice in the TTL also contributes to the amount of water vapor entering the stratosphere (Nielsen et al., 2007; Corti et al., 2008; Steinwagner et al., 2010; Dessler et al., 2016; Ueyama et al., 2015, 2018 Schoeberl et al., 2014, 2018; Ye et al., 2018). To better understand this, we analyze a chemistry-climate model where evaporation of convective ice is known to add water to the TTL (Dessler et al., 2016; Ye et al., 2018). Previous work (Ye et al., 2018) has shown that the behavior of the GEOSCCM in the TTL is reasonable and agrees well with observations. Comparisons with Cloud-Aerosol Lidar with Orthogonal Polarization (CALIOP) observations (Hu et al., 2009; Liu et al., 2009; Vaughan et al., 2009; Winker et al., 2009, 2010; Young and Vaughan, 2009; Avery et al., 2012; Heymsfield et al., 2014) show that the GEOSCCM IWC has too much ice in the TTL, but we used two sensitivity tests to show that our results are not sensitive too these disagreements.

Using a version of the trajectory model driven by GEOSCCM meteorology that includes evaporation of GEOSCCM convective ice, we obtained a more accurately simulated seasonal cycle of the 100-hPa water vapor between 10°N-40°N and the hemispheric asymmetry compared to the GEOSCCM. We showed results where the GEOSCCM's IWC is reduced to 20% of the original value, and that did not affect our conclusions. In addition, our results are also not sensitive to GEOSCCM putting convective ice too high in altitude (above 90 hPa). In these runs, adding convective ice to the trajectory model increases the 100-hPa 10°N-40°N seasonal maximum by 1.65 ppmv (44%), and increases the seasonal amplitude by 1.03 ppmv (112%). We note that our estimate of convective moistening in the NH subtropical seasonal cycle in the GEOSCCM is larger than the value produced by previous studies based on observations (e.g., Ueyama et al., 2018). This could be due to overestimates of IWC by the GEOSCCM or because the instant dehydration scheme and instant ice evaporation scheme we use lead to a greater convective impact on water vapor values overall. Therefore we regard our results as providing insight for understanding the observations, but we caution against assuming that the numbers we calculate for ice evaporation in the GEOSCCM are quantitatively accurate estimates of our atmosphere's values.

The majority of the convective moistening at 100-hPa and between 10°N-40°N is contributed by convective ice evaporation in the 10°N-40°N latitudinal range during boreal summer. The maximum convective ice evaporation in this region is due to available convective ice and relative humidity low enough to allow it to evaporate (Dessler and Sherwood, 2004). Ice evaporation between 10°N-40°N contributes to 63% and 59% of the net convective moistening in the 100-hPa 10°N-40°N water vapor seasonal maximum value and seasonal amplitude. Between 10°N-40°N, the Asian monsoon region plays the most important role in convective moistening by ice evaporation. Convective ice evaporation in other regions, including the deep

Deleted: (e.g. Rosenlof, 1997; Randel et al., 1998, 2001, and references therein). Trajectory models that only regulate TTL

Deleted: reanalysis

Deleted: Recent studies suggested that evaporation of convectively injected ice in the TTL also contributes to the amount of water vapor entering the stratosphere (Nielsen et al., 2007; Corti et al., 2008; Steinwagner et al., 2010; Ueyama et al., 2015; Dessler et al., 2016; Schoeberl et al., 2014, 2018; Ye et al., 2018). To better understand this, we analyse a chemistry-climate model where evaporation of convective ice is known to add water to the TTL

Deleted: behaviour

Deleted: LS water vapor and convection in the

Deleted: are

Deleted: agree

Deleted: We extend that here by showing that there is general agreement between GEOSCCM convective ice water content (IWC) and IWC from

Deleted: .¶

Deleted: convectively lofted

Deleted: LS

Deleted: Convective ice evaporation in this

Deleted: maximum value of the

Deleted: water vapor

Deleted: cycle

Deleted: 9

Deleted: 47%)

Deleted: 10°N-40°N

Deleted: 26

Deleted: 123%) compared to standard model. ¶
A major part of the

Deleted: 10°N-40°N water vapor seasonal cycle

Deleted: IWC

Deleted: 1.46 ppmv (71%)

Deleted: 1.09 ppmv (86%)

Deleted: is

Deleted: region for convective ice evaporation and tropics between 10°S-10°N, has a smaller influence in 100-hPa water vapor between 10°N-40°N. However, since the GEOSCCM underestimates the observed convective ice over the North American monsoon above 120 hPa (not shown), it is likely that this causes an underestimation of the moistening effect of convective ice over the North American region. Previous studies showed that the ratio of isotopic water vapor (HDO), an indicator of sublimation of convective ice and in-mixing (e.g., Dessler et al., 2007; Hanisco et al., 2007; Randel et al., 2012), enhances over the American monsoon region during boreal summer, suggesting more convective ice evaporation there (Randel et al., 2012). This paper does not discuss the HDO issue, and more work needs to be done in the future.

To summarize, we find that TTL temperature variations alone cannot explain the seasonal cycle of water vapor at 100 hPa in MLS observations over the NH subtropics, 10°N-40°N (although temperature does explain the seasonal cycle in the tropics, 10°S-10°N and southern subtropics, 10°S-40°S). To try to understand the other mechanisms at work, we analyze a chemistry-climate model, the GEOSCCM, which reproduces the MLS observations and has been shown to accurately simulate the TTL. We find that, in the GEOSCCM, evaporation of convective ice in the TTL is responsible for the larger seasonal cycle in the 100-hPa NH subtropics. We therefore conclude that evaporation of convective ice in the TTL, mainly in boreal summer, is the most likely explanation for the observed larger seasonal cycle in the NH subtropics. We concur that the seasonal cycle of the TTL temperatures is the major driver of the seasonal cycle of water vapor entering the stratosphere, but we find that the contribution from evaporation of convective ice fills in more details of this simple picture. Our findings emphasize the need to better understand and quantify the magnitude and spatial pattern of convective ice evaporation in the TTL.

Deleted: LS water vapor between 10°N-40°N

Deleted: of the TTL

Deleted: northern hemisphere

Deleted: it

Deleted:

Deleted: analyse

Deleted:

Deleted: large

Deleted: GEOSCCM in the northern hemisphere

Deleted:

Deleted: large

Deleted: northern hemisphere

Deleted: tropical LS

Deleted: fill

Data availability. The water vapor observed by MLS is available from https://mls.jpl.nasa.gov/. The ice water content observed by CALIOP is available from https://eosweb.larc.nasa.gov/. The MERRA-2 meteorological fields are available from https://disc.gsfc.nasa.gov/. The ERAi meteorological fields are available from https://www.ecmwf.int/en/forecasts/datasets/reanalysis-datasets/era-interim.

Competing interests. The authors declare that they have no conflict of interest.

Author contribution. Xun Wang performed analysis, and wrote the original draft. Andrew E. Dessler provided the conceptualization, guidance, and editing. Mark R. Schoeberl and Tao Wang contributed to the trajectory model code, methodology, discussion, and editing. Wandi Yu contributed to methodology and discussion.

Acknowledgments. This work was supported by NASA grants NNX16AM15G and 80NSSC18K0134, both to Texas A&M University. We would like to thank Dr. Luke Oman for providing the GEOSCCM meteorological fields used in this study.

References

Avery, M., Winker, D., Heymsfield, A., Vaughan, M., Young, S., Hu, Y. and Trepte, C.: Cloud ice water content retrieved from the CALIOP space-based lidar, Geophys. Res. Lett., 39(5), n/a-n/a, doi:10.1029/2011gl050545, 2012.

Avery, M. A., Davis, S. M., Rosenlof, K. H., Ye, H. and Dessler, A. E.: Large anomalies in lower stratospheric water vapour and ice during the 2015–2016 El Niño, Nat. Geosci., 10(6), 405–409, doi:10.1038/ngeo2961, 2017.

Bacmeister, J. T., Suarez, M. J. and Robertson, F. R.: Rain Reevaporation, Boundary Layer–Convection Interactions, and Pacific Rainfall Patterns in an AGCM, J. Atmos. Sci., 63(12), 3383–3403, doi:10.1175/JAS3791.1, 2006.

Bannister, R. N., O'Neill, A., Gregory, A. R. and Nissen, K. M.: The role of the south-east Asian monsoon and other seasonal features in creating the 'tape-recorder' signal in the Unified Model, Q. J. R. Meteorol. Soc., 130(599), 1531–1554, doi:10.1256/qj.03.106, 2004.

Barahona, D., Molod, A., Bacmeister, J., Nenes, A., Gettelman, A., Morrison, H., Phillips, V. and Eichmann, A.: Development of two-moment cloud microphysics for liquid and ice within the NASA Goddard Earth Observing System Model (GEOS-5), Geosci. Model Dev., 7(4), 1733–1766, doi:10.5194/gmd-7-1733-2014, 2014.

Bian, J., Pan, L. L., Paulik, L., Vömel, H., Chen, H. and Lu, D.: In situ water vapor and ozone measurements in Lhasa and Kunming during the Asian summer monsoon, Geophys. Res. Lett., 39(19), n/a-n/a, doi:10.1029/2012GL052996, 2012.

Bowman, K. P.: Large-scale isentropic mixing properties of the Antarctic polar vortex from analyzed winds, J. Geophys. Res. Atmos., 98(D12), 23013–23027, doi:10.1029/93JD02599, 1993.

Bowman, K. P. and Carrie, G. D.: The mean-meridional transport circulation of the troposphere in an idealized {GCM}, J. Atmos. Sci., 59(9), 1502–1514, doi:10.1175/1520-0469(2002)059<1502:TMMTCO>2.0.CO;2, 2002.

Brewer, A. W.: Evidence for a world circulation provided by the measurements of helium and water vapour distribution in the stratosphere, Q. J. R. Meteorol. Soc., 75(326), 351–363, doi:10.1002/qj.49707532603, 1949.

Corti, T., Luo, B. P., de Reus, M., Brunner, D., Cairo, F., Mahoney, M. J., Martucci, G., Matthey, R., Mitev, V., dos Santos, F. H., Schiller, C., Shur, G., Sitnikov, N. M., Spelten, N., Vössing, H. J., Borrmann, S. and Peter, T.: Unprecedented evidence for deep convection hydrating the tropical stratosphere, Geophys. Res. Lett., 35(10), n/a--n/a, doi:10.1029/2008GL033641, 2008.

Dessler, A. E. and Sherwood, S. C.: Effect of convection on the summertime extratropical lower stratosphere, J. Geophys. Res. Atmos., 109(D23), doi:10.1029/2004JD005209, 2004.

Dessler, A. E., Hanisco, T. F. and Fueglistaler, S.: Effects of convective ice lofting on H 2 O and HDO in the tropical tropopause layer, J. Geophys. Res., 112(D18), D18309, doi:10.1029/2007JD008609, 2007.

Dessler, A. E., Ye, H., Wang, T., Schoeberl, M. R., Oman, L. D., Douglass, A. R., Butler, A. H., Rosenlof, K. H., Davis, S. M. and Portmann, R. W.: Transport of ice into the stratosphere and the humidification of the stratosphere over the 21st century, Geophys. Res. Lett., 43(5), 2323–2329, doi:10.1002/2016GL067991, 2016.

Dethof, A., O'Neill, A., Slingo, J. M. and Smit, H. G. J.: A mechanism for moistening the lower stratosphere involving the Asian summer monsoon, Q. J. R. Meteorol. Soc., 125(556), 1079–1106, doi:10.1002/qj.1999.49712555602, 1999.

Dvortsov, V. L. and Solomon, S.: Response of the stratospheric temperatures and ozone to past and future increases in stratospheric humidity, J. Geophys. Res. Atmos., 106(D7), 7505–7514, doi:10.1029/2000JD900637, 2001.

Fu, R., Hu, Y., Wright, J. S., Jiang, J. H., Dickinson, R. E., Chen, M., Filipiak, M., Read, W. G., Waters, J. W. and Wu, D. L.: Short circuit of water vapor and polluted air to the global stratosphere by convective transport over the Tibetan Plateau, , 103(15), 5664–5669, doi:10.1073/pnas.0601584103, 2006.

Fueglistaler, S.: Stratospheric water vapor predicted from the Lagrangian temperature history of air entering the stratosphere in the tropics, J. Geophys. Res., 110(D8), D08107, doi:10.1029/2004JD005516, 2005.

Fueglistaler, S., Dessler, A. E., Dunkerton, T. J., Folkins, I., Fu, Q. and Mote, P. W.: Tropical tropopause layer, Rev. Geophys., 47, 1–31, doi:10.1029/2008RG000267, 2009.

Gelaro, R., McCarty, W., Suárez, M. J., Todling, R., Molod, A., Takacs, L., Randles, C. A., Darmenov, A., Bosilovich, M. G., Reichle, R., Wargan, K., Coy, L., Cullather, R., Draper, C., Akella, S., Buchard, V., Conaty, A., da Silva, A. M., Gu, W., Kim, G.-K., Koster, R., Lucchesi, R., Merkova, D., Nielsen, J. E., Partyka, G., Pawson, S., Putman, W., Rienecker, M., Schubert, S. D., Sienkiewicz, M. and Zhao, B.: The Modern-Era Retrospective Analysis for Research and Applications, Version 2 (MERRA-2), J. Clim., 30(14), 5419–5454, doi:10.1175/JCLI-D-16-0758.1, 2017.

Gent, P. R., Danabasoglu, G., Donner, L. J., Holland, M. M., Hunke, E. C., Jayne, S. R., Lawrence, D. M., Neale, R. B., Rasch, P. J., Vertenstein, M., Worley, P. H., Yang, Z.-L. and Zhang, M.: The Community Climate System Model Version 4, J. Clim., 24(19), 4973–4991, doi:10.1175/2011JCLI4083.1, 2011.

Gettelman, A., Kinnison, D. E., Dunkerton, T. J. and Brasseur, G. P.: Impact of monsoon circulations on the upper troposphere and lower stratosphere, J. Geophys. Res. Atmos., 109(D22), doi:10.1029/2004JD004878, 2004.

Hanisco, T. F., Moyer, E. J., Weinstock, E. M., St. Clair, J. M., Sayres, D. S., Smith, J. B., Lockwood, R., Anderson, J. G., Dessler, A. E., Keutsch, F. N., Spackman, J. R., Read, W. G. and Bui, T. P.: Observations of deep convective influence on stratospheric water vapor and its isotopic composition, Geophys. Res. Lett., 34(4), L04814, doi:10.1029/2006GL027899, 2007.

Heymsfield, A., Winker, D., Avery, M., Vaughan, M., Diskin, G., Deng, M., Mitev, V. and Matthey, R.: Relationships between Ice Water Content and Volume Extinction Coefficient from In Situ Observations for Temperatures from 0° to −86°C: Implications for Spaceborne Lidar Retrievals*, J. Appl. Meteorol. Climatol., 53(2), 479–505, doi:10.1175/JAMC-D-13-087.1, 2014.

Holton, J. R., Haynes, P. H., McIntyre, M. E., Douglass, A. R., Rood, R. B. and Pfister, L.: Stratosphere-troposphere exchange, Rev. Geophys., 33(4), 403, doi:10.1029/95RG02097, 1995.

Hu, Y., Winker, D., Vaughan, M., Lin, B., Omar, A., Trepte, C., Flittner, D., Yang, P., Nasiri, S. L., Baum, B., Holz, R., Sun, W., Liu, Z., Wang, Z., Young, S., Stamnes, K., Huang, J. and Kuehn, R.: CALIPSO/CALIOP Cloud Phase Discrimination Algorithm, J. Atmos. Ocean. Technol., 26(11), 2293–2309, doi:10.1175/2009JTECHA1280.1, 2009.

Jackson, D. R., Driscoll, S. J., Highwood, E. J., Harries, J. E. and Russell, J. M.: Troposphere to stratosphere transport at low latitudes as studies using HALOE observations of water vapour 1992–1997, Q. J. R. Meteorol. Soc., 124(545), 169–192, doi:10.1002/qj.49712454508, 1998.

James, R., Bonazzola, M., Legras, B., Surbled, K. and Fueglistaler, S.: Water vapor transport and dehydration above convective outflow during Asian monsoon, Geophys. Res. Lett., 35(20), doi:10.1029/2008GL035441, 2008.

Jensen, E. J., Diskin, G., Lawson, R. P., Lance, S., Bui, T. P., Hlavka, D., McGill, M., Pfister, L., Toon, O. B. and Gao, R.: Ice nucleation and dehydration in the Tropical Tropopause Layer, Proc. Natl. Acad. Sci., 110(6), 2041–2046, doi:10.1073/pnas.1217104110, 2013.

Kärcher, B., Hendricks, J. and Lohmann, U.: Physically based parameterization of cirrus cloud formation for use in global atmospheric models, J. Geophys. Res., 111(D1), D01205, doi:10.1029/2005JD006219, 2006.

Lambert, A., Read, W. G., Livesey, N. J., Santee, M. L., Manney, G. L., Froidevaux, L., Wu, D. L., Schwartz, M. J., Pumphrey, H. C., Jimenez, C., Nedoluha, G. E., Cofield, R. E., Cuddy, D. T., Daffer, W. H., Drouin, B. J., Fuller, R. A., Jarnot, R. F., Knosp, B. W., Pickett, H. M., Perun, V. S., Snyder, W. V, Stek, P. C., Thurstans, R. P., Wagner, P. A., Waters, J. W., Jucks, K. W., Toon, G. C., Stachnik, R. A., Bernath, P. F., Boone, C. D., Walker, K. A., Urban, J., Murtagh, D., Elkins, J. W. and Atlas, E.: Validation of the Aura Microwave Limb Sounder middle atmosphere water vapor and nitrous oxide measurements, J. Geophys. Res. Atmos., 112(D24), D24S36, doi:10.1029/2007JD008724, 2007.

Liu, Z., Vaughan, M., Winker, D., Kittaka, C., Getzewich, B., Kuehn, R., Omar, A., Powell, K., Trepte, C. and Hostetler, C.: The CALIPSO Lidar Cloud and Aerosol Discrimination: Version 2 Algorithm and Initial Assessment of Performance, J. Atmos. Ocean. Technol., 26(7), 1198–1213, doi:10.1175/2009JTECHA1229.1, 2009.

Livesey, N. J., Read, W. G., Wagner, P. A., Froidevaux, L., Lambert, A., Manney, G. L., Millán-Valle, L. F., Pumphrey, H. C., Santee, M. L., Schwartz, M. J., Wang, S., Fuller, R. A., Jarnot, R. F., Knosp, B. W., and Martinez, E.: Earth Observing System (EOS) Aura Microwave Limb Sounder (MLS), Version 4.2x Level 2 data quality and description document, Tech. Rep. JPL D-33509, Tech. Rep. version 4.2x-3.0, NASA Jet Propulsion Laboratory, 2017.

Luo, J., Pan, L. L., Honomichl, S. B., Bergman, J. W., Randel, W. J., Francis, G., Clerbaux, C., George, M., Liu, X. and Tian, W.: Space–time variability in UTLS chemical distribution in the Asian summer monsoon viewed by limb and nadir satellite sensors, Atmos. Chem. Phys., 18(16), 12511–12530, doi:10.5194/acp-18-12511-2018, 2018.

Molod, A., Takacs, L., Suarez, M., Bacmeister, J., Song, I.-S., and Eichmann, A.: The GEOS-5 atmospheric general circulation model: Mean climate and development from MERRA to Fortuna, Technical Report Series on Global Modeling and Data Assimilation Volume 28, NASA Goddard Space Flight Center, 2012.

Molod, A., Takacs, L., Suarez, M. and Bacmeister, J.: Development of the GEOS-5 atmospheric general circulation model: evolution from MERRA to MERRA2, Geosci. Model Dev., 8(5), 1339–1356, doi:10.5194/gmd-8-1339-2015, 2015.

Mote, P. W., Rosenloh, K. H., Holton, J. R., Harwood, R. S. and Waters, J. W.: Seasonal variations of water vapor in the tropical lower stratosphere, Geophys. Res. Lett., 22(9), 1093–1096, doi:10.1029/95GL01234, 1995.

Mote, P. W., Rosenlof, K. H., McIntyre, M. E., Carr, E. S., Gille, J. C., Holton, J. R., Kinnersley, J. S., Pumphrey, H. C., Russell III, J. M. and Waters, J. W.: An atmospheric tape recorder: The imprint of tropical tropopause temperatures on stratospheric water vapor, J. Geophys. Res., 101(D2), 3989–4006, doi:10.1029/95JD03422, 1996.

Moyer, E. J., Irion, F. W., Yung, Y. L. and Gunson, M. R.: ATMOS stratospheric deuterated water and implications for troposphere-stratosphere transport, Geophys. Res. Lett., 23(17), 2385–2388, doi:10.1029/96GL01489, 1996.

Deleted: Moorthi, S. and Suarez, M. J.: Relaxed Arakawa-Schubert. A Parameterization of Moist Convection for General Circulation Models, Mon. Weather Rev., 120(6), 978–1002, doi:10.1175/1520-0493(1992)120<0978:RASAPO>2.0.CO;2, 1992.

Murphy, D. M. and Koop, T.: Review of the vapour pressures of ice and supercooled water for atmospheric applications, Q. J. R. Meteorol. Soc., 131(608), 1539–1565, doi:10.1256/qj.04.94, 2005.

Nielsen, J. K., Larsen, N., Cairo, F., Donfrancesco, G. Di, Rosen, J. M., Durry, G., Held, G. and Pommereau, J.-P.: Solid particles in the tropical lowest stratosphere, Atmos. Chem. Phys., 7(3), 685–695, doi:10.5194/acp-7-685-2007, 2007.

Oman, L. D. and Douglass, A. R.: Improvements in total column ozone in GEOSCCM and comparisons with a new ozone-depleting substances scenario, J. Geophys. Res. Atmos., 119(9), 5613–5624, doi:10.1002/2014JD021590, 2014.

Pan, L., Solomon, S., Randel, W., Lamarque, J.-F., Hess, P., Gille, J., Chiou, E.-W. and McCormick, M. P.: Hemispheric asymmetries and seasonal variations of the lowermost stratospheric water vapor and ozone derived from SAGE II data, J. Geophys. Res. Atmos., 102(D23), 28177–28184, doi:10.1029/97JD02778, 1997.

Pan, L. L., Hintsa, E. J., Stone, E. M., Weinstock, E. M. and Randel, W. J.: The seasonal cycle of water vapor and saturation vapor mixing ratio in the extratropical lowermost stratosphere, J. Geophys. Res. Atmos., 105(D21), 26519–26530, doi:10.1029/2000JD900401, 2000.

Pan, L. L., Honomichl, S. B., Kinnison, D. E., Abalos, M., Randel, W. J., Bergman, J. W. and Bian, J.: Transport of chemical tracers from the boundary layer to stratosphere associated with the dynamics of the Asian summer monsoon, J. Geophys. Res. Atmos., 121(23), 14,159-14,174, doi:10.1002/2016JD025616, 2016.

Park, M., Randel, W. J., Kinnison, D. E., Garcia, R. R. and Choi, W.: Seasonal variation of methane, water vapor, and nitrogen oxides near the tropopause: Satellite observations and model simulations, J. Geophys. Res. Atmos., 109(D3), n/a-n/a, doi:10.1029/2003JD003706, 2004.

Park, M., Randel, W. J., Gettelman, A., Massie, S. T. and Jiang, J. H.: Transport above the Asian summer monsoon anticyclone inferred from Aura Microwave Limb Sounder tracers, J. Geophys. Res. Atmos., 112(D16), 2007.

Pawson, S., Stolarski, R. S., Douglass, A. R., Newman, P. A., Nielsen, J. E., Frith, S. M. and Gupta, M. L.: Goddard Earth Observing System chemistry-climate model simulations of stratospheric ozone-temperature coupling between 1950 and 2005, J. Geophys. Res., 113(D12), D12103, doi:10.1029/2007JD009511, 2008.

Ploeger, F., Günther, G., Konopka, P., Fueglistaler, S., Müller, R., Hoppe, C., Kunz, A., Spang, R., Grooß, J.-U. and Riese, M.: Horizontal water vapor transport in the lower stratosphere from subtropics to high latitudes during boreal summer, J. Geophys. Res. Atmos., 118(14), 8111–8127, doi:10.1002/jgrd.50636, 2013.

Randel, W. J. and Park, M.: Deep convective influence on the Asian summer monsoon anticyclone and associated tracer variability observed with Atmospheric Infrared Sounder (AIRS), J. Geophys. Res., 111(D12), D12314, doi:10.1029/2005JD006490, 2006.

Randel, W. J., Wu, F., Russell, J. M., Roche, A. and Waters, J. W.: Seasonal Cycles and QBO Variations in Stratospheric $CH_4$and H_2O Observed inUARSHALOE Data, J. Atmos. Sci., 55(2), 163–185, doi:10.1175/1520-0469(1998)055<0163:Scaqvi>2.0.Co;2, 1998.

Randel, W. J., Wu, F., Gettelman, A., Russell, J. M., Zawodny, J. M. and Oltmans, S. J.: Seasonal variation of water vapor in the lower stratosphere observed in Halogen Occultation Experiment data, J. Geophys. Res. Atmos., 106(D13), 14313–14325, doi:10.1029/2001jd900048, 2001.

Randel, W. J., Moyer, E., Park, M., Jensen, E., Bernath, P., Walker, K. and Boone, C.: Global variations of HDO and HDO/H 2 O ratios in the upper troposphere and lower stratosphere derived from ACE-FTS satellite measurements, J. Geophys. Res. Atmos., 117(D6), n/a-n/a, doi:10.1029/2011JD016632, 2012.

Randel, W. J., Zhang, K. and Fu, R.: What controls stratospheric water vapor in the NH summer monsoon regions?, J. Geophys. Res. Atmos., 120(15), 7988–8001, doi:10.1002/2015JD023622, 2015.

Rienecker, M.M., Suarez, M.J., Todling, R., Bacmeister, J., Takacs, L., Liu, H.-C., Gu, W., Sienkiewicz, M., Koster, R.D., Gelaro, R., Stajner, I., and Nielsen J.E.: The GEOS-5 data assimilation system—Documentation of versions 5.0.1, 5.1.0, and 5.2.0, Technical Report Series on Global Modeling and Data Assimilation, Volume 27, NASA Goddard Space Flight Center Greenbelt, 2008.

Rosenlof, K. H.: Hemispheric asymmetries in water vapor and inferences about transport in the lower stratosphere, J. Geophys. Res. Atmos., 102(D11), 13213–13234, doi:10.1029/97JD00873, 1997.

Schoeberl, M., Dessler, A., Ye, H., Wang, T., Avery, M. and Jensen, E.: The impact of gravity waves and cloud nucleation threshold on stratospheric water and tropical tropospheric cloud fraction, Earth Sp. Sci., 3(8), 295–305, doi:10.1002/2016EA000180, 2016.

Schoeberl, M. R. and Dessler, A. E.: Dehydration of the stratosphere, Atmos. Chem. Phys., 11(16), 8433–8446, doi:10.5194/acp-11-8433-2011, 2011.

Schoeberl, M. R., Douglass, A. R., Newman, P. A., Lait, L. R., Lary, D., Waters, J., Livesey, N., Froidevaux, L., Lambert, A., Read, W., Filipiak, M. J. and Pumphrey, H. C.: QBO and annual cycle variations in tropical lower stratosphere trace gases from HALOE and Aura MLS observations, J. Geophys. Res. Atmos., 113(D5), n/a-n/a, doi:10.1029/2007JD008678, 2008.

Schoeberl, M. R., Dessler, A. E. and Wang, T.: Modeling upper tropospheric and lower stratospheric water vapor anomalies, Atmos. Chem. Phys., 13(15), 7783–7793, doi:10.5194/acp-13-7783-2013, 2013.

Schoeberl, M. R., Dessler, A. E., Wang, T., Avery, M. A. and Jensen, E. J.: Cloud formation, convection, and stratospheric dehydration, Earth Sp. Sci., 1(1), 1–17, doi:10.1002/2014EA000014, 2014.

Schoeberl, M. R., Jensen, E. J. and Woods, S.: Gravity waves amplify upper tropospheric dehydration by clouds, Earth Sp. Sci., 2(12), 485–500, doi:10.1002/2015EA000127, 2015.

Schoeberl, M. R., Jensen, E. J., Pfister, L., Ueyama, R., Avery, M. and Dessler, A. E.: Convective Hydration of the Upper Troposphere and Lower Stratosphere, J. Geophys. Res. Atmos., 123(9), 4583–4593, doi:10.1029/2018JD028286, 2018.

Schoeberl, M. R., Jensen, E. J., Pfister, L., Ueyama, R., Wang, T., Selkirk, H., Avery, M., Thornberry, T. and Dessler, A. E.: Water Vapor, Clouds, and Saturation in the Tropical Tropopause Layer, J. Geophys. Res. Atmos., 124(7), 3984–4003, doi:10.1029/2018JD029849, 2019.

Schwartz, M. J., Read, W. G., Santee, M. L., Livesey, N. J., Froidevaux, L., Lambert, A. and Manney, G. L.: Convectively injected water vapor in the North American summer lowermost stratosphere, Geophys. Res. Lett., 40(10), 2316–2321, doi:10.1002/grl.50421, 2013.

Solomon, S., Garcia, R. R., Rowland, F. S. and Wuebbles, D. J.: On the depletion of Antarctic ozone, Nature, 321(6072), 755–758, doi:doi:10.1038/321755a0, 1986.

Steinwagner, J., Fueglistaler, S., Stiller, G., von Clarmann, T., Kiefer, M., Borsboom, P.-P., van Delden, A. and Röckmann, T.: Tropical dehydration processes constrained by the seasonality of stratospheric deuterated water, Nat. Geosci., 3, 262, doi:10.1038/ngeo822, 2010.

Ueyama, R., Jensen, E. J., Pfister, L. and Kim, J.-E.: Dynamical, convective, and microphysical control on wintertime distributions of water vapor and clouds in the tropical tropopause layer, J. Geophys. Res. Atmos., 120(19), 10,410-483,500, doi:10.1002/2015JD023318, 2015.

Ueyama, R., Jensen, E. J. and Pfister, L.: Convective Influence on the Humidity and Clouds in the Tropical Tropopause Layer During Boreal Summer, J. Geophys. Res. Atmos., doi:10.1029/2018JD028674, 2018.

Vaughan, M. A., Powell, K. A., Winker, D. M., Hostetler, C. A., Kuehn, R. E., Hunt, W. H., Getzewich, B. J., Young, S. A., Liu, Z. and McGill, M. J.: Fully Automated Detection of Cloud and Aerosol Layers in the CALIPSO Lidar Measurements, J. Atmos. Ocean. Technol., 26(10), 2034–2050, doi:10.1175/2009JTECHA1228.1, 2009.

Van Vuuren, D. P., Edmonds, J., Kainuma, M., Riahi, K., Thomson, A., Hibbard, K., Hurtt, G. C., Kram, T., Krey, V., Lamarque, J.-F. and others: The representative concentration pathways: an overview, Clim. Change, 109, 5–31, doi:10.1007/s10584-011-0148-z, 2011.

Winker, D. M., Vaughan, M. A., Omar, A., Hu, Y., Powell, K. A., Liu, Z., Hunt, W. H. and Young, S. A.: Overview of the CALIPSO Mission and CALIOP Data Processing Algorithms, J. Atmos. Ocean. Technol., 26(11), 2310–2323, doi:10.1175/2009jtecha1281.1, 2009.

Winker, D. M., Pelon, J., Coakley, J. A., Ackerman, S. A., Charlson, R. J., Colarco, P. R., Flamant, P., Fu, Q., Hoff, R. M., Kittaka, C., Kubar, T. L., Le Treut, H., Mccormick, M. P., Mégie, G., Poole, L., Powell, K., Trepte, C., Vaughan, M. A. and Wielicki, B. A.: The CALIPSO Mission, Bull. Am. Meteorol. Soc., 91(9), 1211–1230, doi:10.1175/2010BAMS3009.1, 2010.

Woods, S., Lawson, R. P., Jensen, E., Bui, T. P., Thornberry, T., Rollins, A., Pfister, L. and Avery, M.: Microphysical Properties of Tropical Tropopause Layer Cirrus, J. Geophys. Res. Atmos., 123(11), 6053–6069, doi:10.1029/2017JD028068, 2018.

World Meteorological Organization: Scientific assessment of ozone depletion, Global Ozone Research and Monitoring Project–Report No. 52, Geneva, Switzerland, 2010.

Wright, J. S., Fu, R., Fueglistaler, S., Liu, Y. S. and Zhang, Y.: The influence of summertime convection over Southeast Asia on water vapor in the tropical stratosphere, J. Geophys. Res. Atmos., 116(D12), 1–12, doi:10.1029/2010JD015416, 2011.

Ye, H., Dessler, A. E. and Yu, W.: Effects of convective ice evaporation on interannual variability of tropical tropopause layer water vapor, Atmos. Chem. Phys., 18(7), 4425–4437, doi:10.5194/acp-18-4425-2018, 2018.

Young, S. A. and Vaughan, M. A.: The Retrieval of Profiles of Particulate Extinction from Cloud-Aerosol Lidar Infrared Pathfinder Satellite Observations (CALIPSO) Data: Algorithm Description, J. Atmos. Ocean. Technol., 26(6), 1105–1119, doi:10.1175/2008JTECHA1221.1, 2009.

Table 1: Summary of trajectory model cases

Trajectory Model Cases	Description
ERAi standard trajectory model	Instant dehydration with no convective influence
MERRA-2 standard trajectory model	Instant dehydration with no convective influence
ERAi trajectory with cloud model	Dehydration with the cloud model, but with no convective influence
MERRA-2 trajectory with cloud model	Dehydration with the cloud model, but with no convective influence
GEOSCCM standard trajectory model	Instant dehydration with no convective influence
GEOSCCM ice model	Instant dehydration. Convective ice instantly evaporates to sub-saturated parcels
GEOSCCM 0.2ice model	Instant dehydration. GEOSCCM convective ice input is decreased by 80%. Convective ice instantly evaporates to sub-saturated parcels
GEOSCCM ice model below 90 hPa	Instant dehydration. Convective ice evaporation above the 90-hPa surface is not allowed

Deleted: ice

Deleted: + τ

Deleted: and relaxes the RH towards pre-set threshold with an e-folding time scale τ

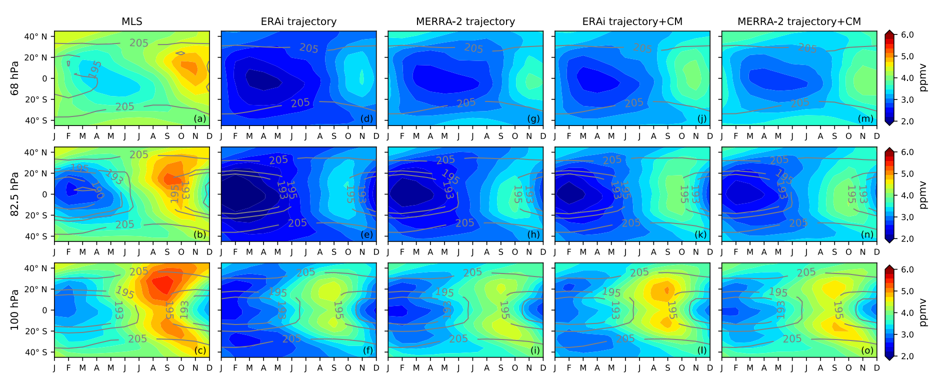

Figure 1: Zonal mean seasonal cycle water vapor (ppmv, color shading) and temperature (K, contour lines) between 40°S - 40°N from (a)-(c) MLS, (d)-(f) ERAi trajectory model, (g)-(i) MERRA-2 trajectory model, (j)-(l) ERAi trajectory model with the cloud model, and (m)-(o) MERRA-2 trajectory model with the cloud model at 68 hPa (top row), 82.5 hPa (middle row) and 100 hPa (bottom row).

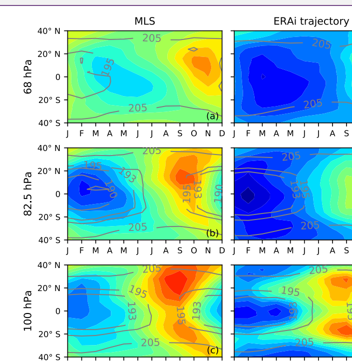

Deleted:

Deleted: 1

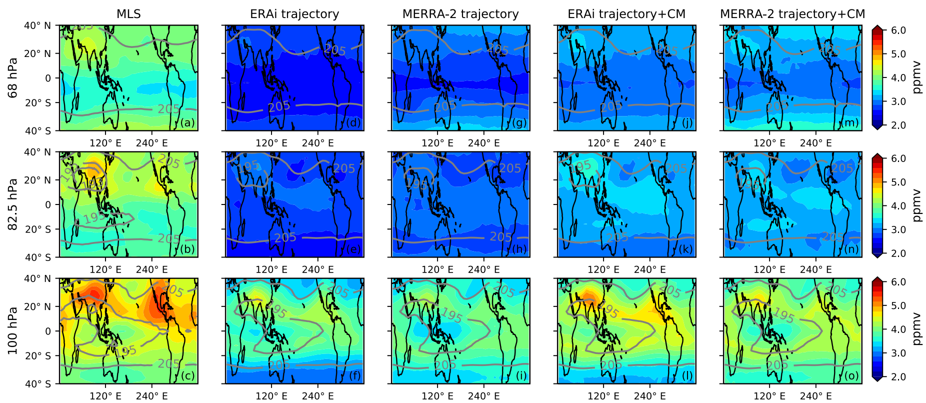

Deleted:

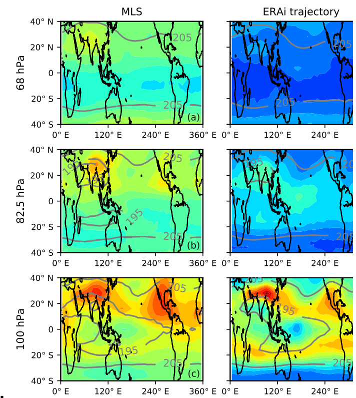

Figure 2: JJA water vapor (ppmv, color shading) and temperature (K, contour lines) between 40°S - 40°N from (a)-(c) MLS, (d)-(f) ERAi trajectory model, (g)-(i) MERRA-2 trajectory model, (j)-(l) ERAi trajectory model with the cloud model, and (m)-(o) MERRA-2 trajectory model with the cloud model at 68 hPa (top row), 82.5 hPa (middle row) and 100 hPa (bottom row).

Deleted: 2

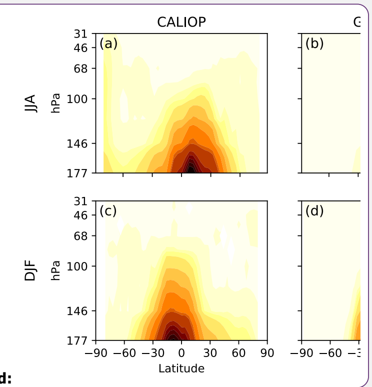

Deleted:

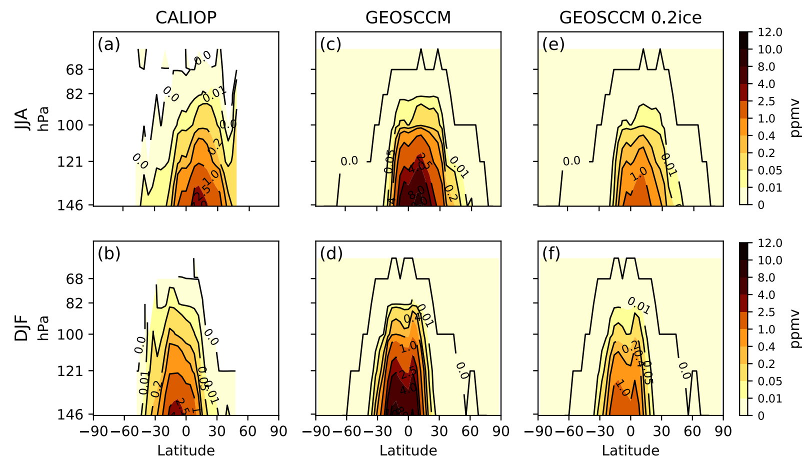

Figure 3. Zonal mean convective IWC (ppmv) from CALIOP and GEOSCCM above 146 hPa. The CALIOP ice data is averaged over JJA (top row) and DJF (bottom row) from 200805 – 201312. For CALIOP data (a and b), we show the ice from all clouds minus the ice from cirrus clouds, which is a rough estimate of convective ice in the TTL region. For GEOSCCM ice, we show convective ice (c and d). To better match the tropical average CALIOP ice field above 120 hPa, we decrease the GEOSCCM ice by 80% (0.2ice) and show them in panels e and f. Note we use a nonlinear color scale.

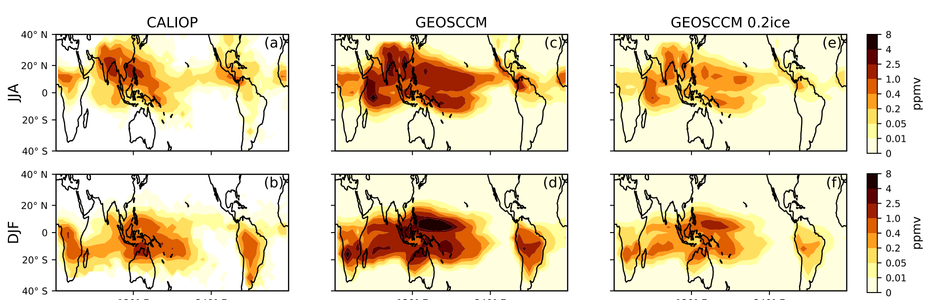

Figure 4. Same as Fig. 3, but for convective IWC (ppmv) averaged between 121-82.5 hPa During JJA and DJF.

Deleted: 2007-2017 …onal mean convective IWC (mg m-3…pmv) from (left) …ALIOP and (right) …EOSCCM for June-July-August (…bove 146 hPa. The CALIOP ice data is averaged over JJA, …(top row),… and for December-January-February (…JF, …(bottom row). ... [3]

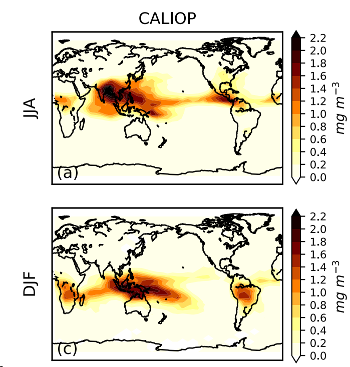

Deleted:

Deleted: 2007-2017…ame as Fig. 3, but for convective IWC (mg m-3) from (left) CALIOP and (right) GEOSCCM …pmv) averaged between 177-68…21-82.5 hPa for June-July-August (…uring JJA, top row), and for December-January-February (…and DJF, bottom row).

Page Break ... [4]

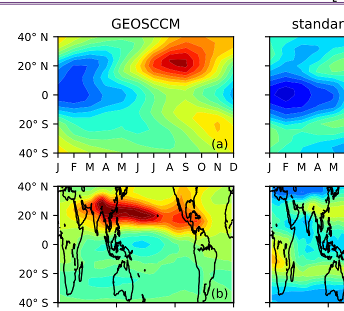

Deleted:

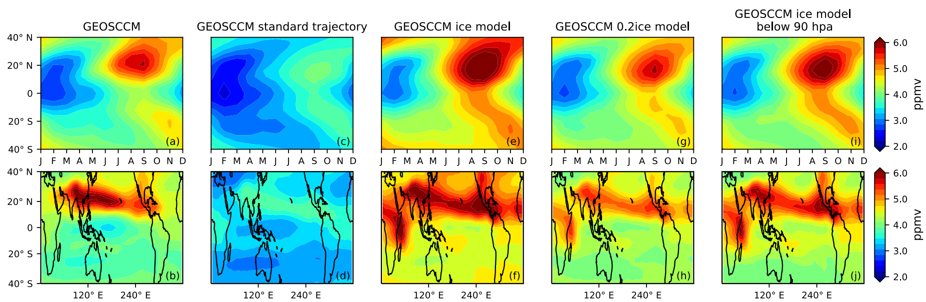

Figure 5. Top panel: Zonal mean seasonal cycle of 100-hPa water vapor (ppmv) between 40°S - 40°N from (a) GEOSCCM, (c) GEOSCCM standard model, (e) GEOSCCM ice model (g) GEOSCCM 0.2ice model, and (i) GEOSCCM ice model with ice below 90 hPa. Bottom panel: JJA 100-hPa water vapor (ppmv) between 40°S - 40°N from (b) GEOSCCM, (d) GEOSCCM standard model, (f) GEOSCCM ice model (h) GEOSCCM 0.2ice model, and (j) GEOSCCM ice model with ice below 90 hPa.

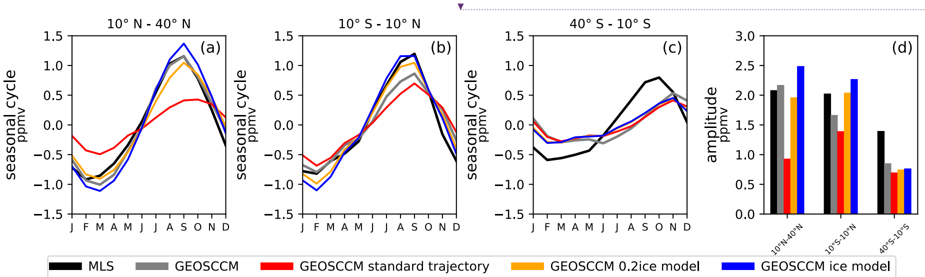

Figure 6. Seasonal cycles of water vapor at 100 hPa averaged between (a) 10°N-40°N, (b) 10°S-10°N, and (c) 40°S-10°S and their (d) seasonal amplitudes from GEOSCCM, GEOSCCM standard model, GEOSCCM ice model, and GEOSCCM 0.2ice model. We have subtracted the annual mean from each data set.

Deleted: g)

Deleted: a finite time

Deleted: evaporation scheme.

Deleted: ice

Deleted: h)

Deleted: a finite time

Deleted: evaporation scheme.

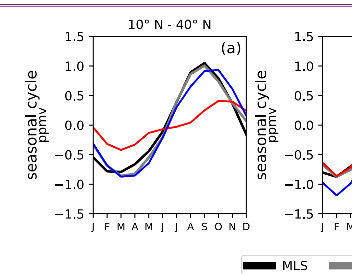

Deleted:

Deleted: and

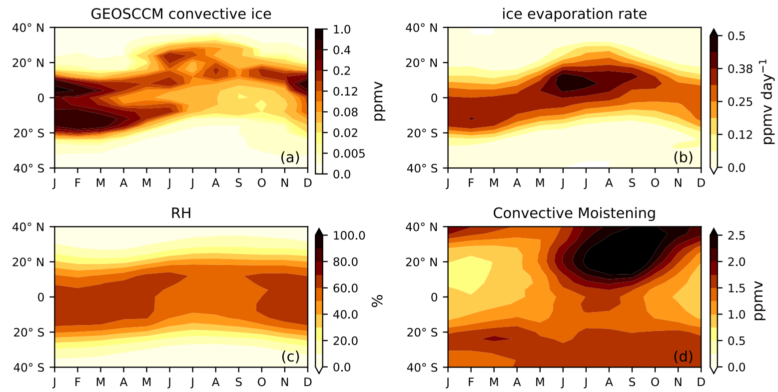

Figure 7. (a) Zonal mean seasonal cycle of 100-hPa convective ice (ppmv) from GEOSCCM. Note the color scale is nonlinear. (b) Zonal mean seasonal cycle of 100-hPa evaporation rate (ppmv day-1) from the GEOSCCM ice model. (c) Zonal mean seasonal cycle of relative humidity (%) with respect to ice at 100 hPa from GEOSCCM. (d) Zonal mean seasonal cycle of net convective moistening (ppmv) at 100 hPa from the ice model. The quantity net convective moistening is the difference between water vapor values from the ice model and standard model.

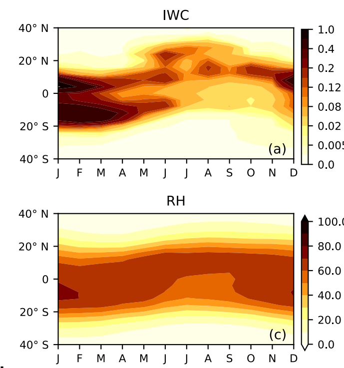

Deleted:

Deleted: lofted IWC

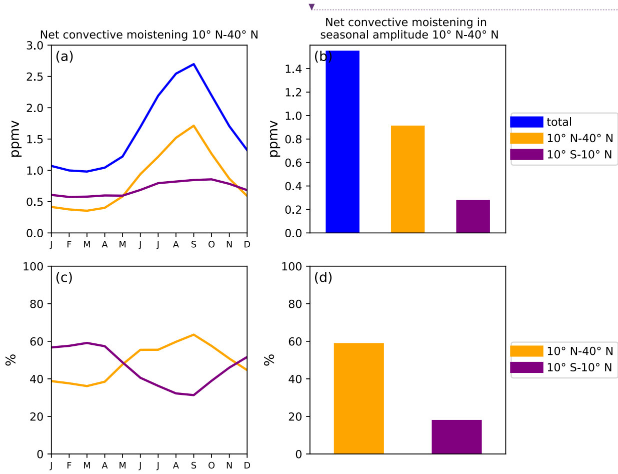

Figure 8. (a) Net convective moistening (ppmv) in the 10°N-40°N water vapor seasonal cycle and the portions (ppmv) contributed by convective ice evaporation over 10°S-10°N and 10°N-40°N. (b) Net convective moistening (ppmv) in the 10°N-40°N water vapor seasonal amplitude and the portions (ppmv) contributed by convective ice evaporation over 10°S-10°N and 10°N-40°N. (c)-(d) Percentage of net convective moistening in the 10°N-40°N water vapor seasonal cycle and seasonal amplitude contributed by convective ice evaporation over 10°S-10°N and 10°N-40°N. The percentage is net convective moistening contributed by 10°S-10°N or 10°N-40°N region divided by the total net convective moistening.

Deleted:

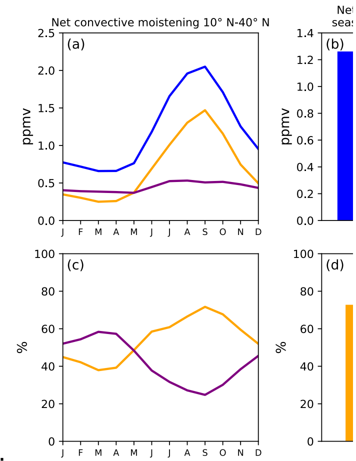

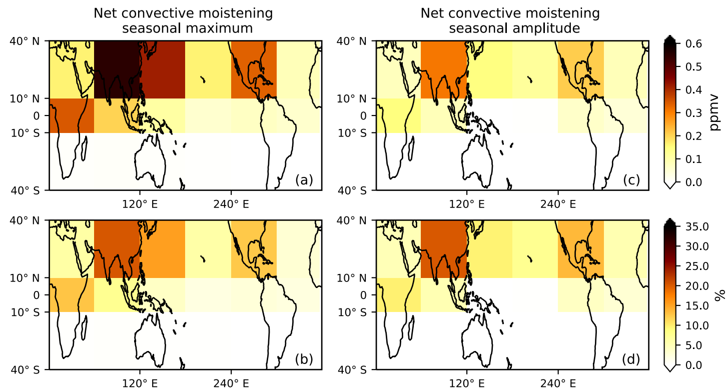

Figure 9. Portions of net convective moistening (ppmv) in the (a) maximum value and (b) seasonal amplitude of the 10°N-40°N water vapor seasonal cycle contributed by 12 equal-area box regions between 10°S-40°N. (c) and (d): Same as (a) and (b), but for the percentage of net convective moistening contributed by the 12 equal-area box regions.

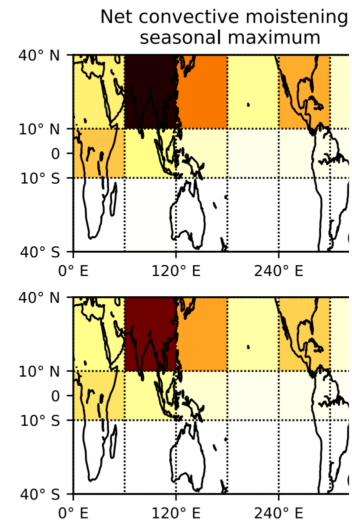

Deleted: